



Timing and pathways of East Antarctic Ice Sheet retreat

Lindsay O. Prothro ^{a, b, *}, Wojciech Majewski ^c, Yusuke Yokoyama ^d, Lauren M. Simkins ^e, John B. Anderson ^a, Masako Yamane ^f, Yosuke Miyairi ^d, Naohiko Ohkouchi ^g

^a Rice University, USA

^b Texas A&M University – Corpus Christi, USA

^c Institute of Paleobiology, Polish Academy of Sciences, Poland

^d University of Tokyo, Japan

^e University of Virginia, USA

^f Nagoya University, Japan

^g JAMSTEC, Japan



ARTICLE INFO

Article history:

Received 28 July 2019

Received in revised form

24 December 2019

Accepted 6 January 2020

Available online 16 January 2020

Keywords:

Ross sea

Last glacial maximum

Glacial history

Sedimentology

Geomorphology

Radiocarbon

ABSTRACT

A lack of reliable chronology often leaves Antarctic ice sheet reconstructions incomplete. Despite being the most heavily investigated region of the Antarctic continental shelf, the post-Last Glacial Maximum (LGM) record of marine-based ice sheet dynamics in the Ross Sea has remained largely elusive and at odds with fringing terrestrial records of ice sheet decay. Issues with radiocarbon dating stem primarily from poorly preserved carbonate, contamination by glacially-recycled carbon, and insufficient consideration for glacial geomorphic context and sedimentary facies. We assess nearly 70 newly acquired and more than 200 published radiocarbon ages in the context of a consistent sedimentary facies and geomorphic framework to interpret the timing of the local glacial maximum and subsequent retreat of the East Antarctic Ice Sheet (EAIS) in the Ross Sea and potential causes of retreat. Compound-specific radiocarbon ages help to provide good constraints on open marine onset, and we demonstrate that, with proper corrections and considerations, acid insoluble organic (AIO) radiocarbon ages can be reliable in open marine sediments and carbonate ages can be reliable in grounding-zone proximal sediments. We find that the ice flowing through Pennell and JOIDES troughs remained at maximum extent for approximately 10,000 years before retreating at 15.1 and 13 cal ka BP, respectively. An ice shelf covered the outer continental shelf until ~9.5 cal ka BP, after which it collapsed in JOIDES Trough, creating deep iceberg furrows. Retreat through Pennell Trough was more episodic, marked by grounding-zone wedges that backstep upstream and onto lateral banks creating deglacial emergent ice rises. As ice retreated from ~9 to ~4 cal ka BP, there was considerable reorganization of drainage and at least one episode of readvance through southern JOIDES Trough that began drawdown of terrestrial ice near Ross Island at ~7.8 cal ka BP. The ice shelf appears to have retreated to a near-present configuration by 2 cal ka BP. However, due to inconsistencies in calendar ages, grounding line position must be inferred from relative chronology based on glacial landforms, which suggests grounded ice retreated nearly to Drygalski Ice Tongue and lingered atop Crary Bank where it was maintained by ice from David Glacier. Our reconstruction further suggests that the EAIS in the western Ross Sea was not a discernible contributor to Meltwater Pulse 1A, but likely contributed to eustatic sea level rise well through the middle—perhaps even late—Holocene.

© 2020 Elsevier Ltd. All rights reserved.

1. Introduction

Perhaps the most concerning possible outcome of future climate change is large-scale mass wasting of the Antarctic Ice Sheet which

is the largest potential contributor to sea-level rise. The rate and location of ice mass loss impacts how coastal communities will be affected by changing sea levels (e.g., Hauer et al., 2016; Schuerch et al., 2018), thus making studies of vulnerable ice sheet sectors and their sensitivity to a range of forcings critical. The Antarctic ice sheets could add 0.1–1 m to global mean sea level (GMSL) by the end of the century and anywhere from 0.2 to 15 m by 2500 (Colledge et al., 2015; Ritz et al., 2015; Winkelmann et al., 2015;

* Corresponding author. Rice University, USA.

E-mail address: lindsay.prothro@tamu.edu (L.O. Prothro).

(DeConto and Pollard, 2016), at times contributing to global rates of rise up to 6 cm yr⁻¹ (DeConto and Pollard, 2016). Because large sectors are resting on a bed above sea level, the East Antarctic Ice Sheet (EAIS) is colloquially considered less vulnerable to climate change than the West Antarctic Ice Sheet (WAIS). However, the EAIS holds an order of magnitude higher sea level equivalent (e.g., Fretwell et al., 2013) with large sectors that are marine-based and sensitive to climate change (Golledge et al., 2017; Gulick et al., 2017; Wilson et al., 2018).

Our understanding of ice margins over both large areas and extended lengths of time can be improved by examining the geologic history as recorded by geomorphic features and sediment cores from deglaciated continental shelves, leading to better-tested and more representative ice sheet models. Despite the utility of geologic observations, ice-sheet extent and the timing of retreat events in the paleo-record is unknown or disputed for much of the Antarctic Ice Sheet, including its retreat from the continental shelf following the Last Glacial Maximum (LGM; 26.5–19 ka BP; Clark et al., 2009). Contention between reconstructions is due largely to difficulties in obtaining accurate radiocarbon dates as a result of a poorly constrained marine reservoir effect, bias from reworked carbon, and uncertainty in glacial-retreat sediment facies (e.g., Andrews et al., 1999; Licht et al., 1999; Prothro et al., 2018).

In spite of such difficulties, the consensus is that the ice sheet sectors did not reach maximum extent synchronously during the LGM, nor did they retreat at the same time (Anderson et al., 2002; Livingstone et al., 2012; Bentley et al., 2014; Yokoyama et al., 2018) or in the same manner (Simkins et al., 2018). This type of variability in contemporary systems has been attributed to local factors, such as bed physiography (Alley et al., 2007; Schoof, 2007), intrusion of warm ocean currents (Shepherd et al., 2004), and variability in atmospheric and precipitation regimes in the respective catchment areas (Morris and Vaughan, 2003; Mayewski et al., 2009).

To begin to understand a comprehensive retreat history of any drainage basin, an integrated analysis of geomorphology, sedimentology, and micropaleontology should be carried out for as many sediment cores as possible to develop a holistic reconstruction and assess the causes of retreat, rather than basing regional-scale reconstructions on very local sedimentological observations. We explore the post-LGM retreat history of EAIS in the western Ross Sea (Fig. 1), where geomorphic reconstructions suggest diachronous and varying styles of ice stream retreat (Halberstadt et al., 2016). Until now, however, this retreat model has not been constrained by age data. Furthermore, the marine record of ice retreat in the Ross Sea has often been shown to be at odds with the terrestrial records of grounded ice retreat (e.g., Conway et al., 1999). Our protocol of establishing geomorphic context and then analyzing sedimentology and micropaleontology is meant to (1) facilitate confidence in interpreting sediment facies, (2) better understand viability in new and previously reported marine radiocarbon dates, and (3) highlight pathways and drivers of retreating ice, thus solidifying the marine record. We employ three different dating methods (acid insoluble organic, carbonate, and compound-specific) and evaluate ages with respect to our facies model, then place them into a standardized ranking system. From these combined investigations, we seek to improve the deglacial record of the western Ross Sea, provide a reference of meaningful published ages for future studies, and establish new practices for conducting chronological reconstructions in glacial settings.

2. Regional background

The Ross Sea (Fig. 1) is the location of the richest collection of marine sediment cores, multibeam bathymetric data, and seismic records around Antarctica. On the continental shelf, six troughs

mark the former paths of at least seven paleo-ice streams and demonstrate the glaciological complexity of this region. Particularly important for reconstructions in the western Ross Sea is identification of glacial lineations as paleoflow indicators and grounding-line landforms, such as grounding-zone wedges and recessional moraines, as marking pathways of grounding-line retreat (Fig. 2; Halberstadt et al., 2016; Lee et al., 2017; Simkins et al., 2018; Greenwood et al., 2018). Grounding-zone wedges (Fig. 3) are wedge-shaped features that record phases of grounding line position stability (Batchelor and Dowdeswell, 2015; Simkins et al., 2018). Recessional moraines are more-or-less symmetrical features that record relatively short pauses in ice margin retreat (Simkins et al., 2018). Moraines are generally thought to be created by deformational push processes of proglacial sediments (Boulton, 1986; Ottesen and Dowdeswell, 2006) and/or through subglacial sediment transport to the grounding line (Ottesen et al., 2005; Todd et al., 2007), similar to grounding-zone wedges (Larter and Vanneste, 1995; Anderson, 1999; Dowdeswell and Fugelli, 2012). Simkins et al. (2018), however, find evidence of deformation and deposition as formative processes in both types of grounding-line landforms in the Ross Sea. The advent of improved high-frequency CHIRP seismic and advanced multibeam swath bathymetry, in conjunction with legacy side-scan sonar records, has allowed imaging of small grounding-zone wedges and moraines that were not observed in previous studies (e.g. Shipp et al., 1999), yielding a more detailed record of ice sheet retreat in the western Ross Sea (Halberstadt et al., 2016; Lee et al., 2017; Simkins et al., 2018; Greenwood et al., 2018).

2.1. Sediment facies and stratigraphy

Sediments from the Ross Sea can generally be separated into six primary sediment facies (Prothro et al., 2018), including Facies 1 (till), Facies 2 (proximal glacimarine sediment gravity flows), Facies 3 (proximal glacimarine basal meltout), Facies 4 (meltwater deposits), Facies 5 (open marine), and Facies 6 (residual glacimarine). Facies 1–5 are well-represented in the study area and are used to interpret radiocarbon ages reported in this and previous studies, but Facies 6 is not present in cores relevant to this study. All facies are presented within the context of geomorphic setting, which has previously been shown to exert some control on stratigraphic successions (Prothro et al., 2018), discussed further in Section 2.2.

Facies 1 (till) is pebble-bearing and has a sandy silt matrix that is very poorly sorted (according to Folk and Ward, 1957 classification) but is homogenous downcore both mineralogically and texturally (Anderson et al., 1980; Anderson, 1999; McGlennan et al., 2017; Prothro et al., 2018; Halberstadt et al., 2018) and foraminifera are either absent from the facies or contain a significant reworked fraction (Licht et al., 1999; Majewski et al., 2018; Prothro et al., 2018). This facies is recovered in cores obtained from subglacial features such as glacial lineations and grounding-zone wedge topsets.

Facies 2 (proximal glacimarine sediment gravity flows) was collected from grounding-zone wedge foresets and toes, consisting of a diamicton with a fine matrix composed of very poorly sorted sandy silt. While it sometimes displays downcore homogeneity similar to till, Facies 2 occasionally shows variability in grain size distribution downcore, leading Prothro et al. (2018) to conclude the deposit is a result of slumps and debris flows on the proglacial lee slope of grounding-zone wedges. Because this deposit originates from the subglacial environment, clearly reworked foraminifera are present. However, this facies contains a more dominant presence of well-preserved calcareous benthic foraminifera (Fig. 4; Majewski et al., 2018; Prothro et al., 2018).

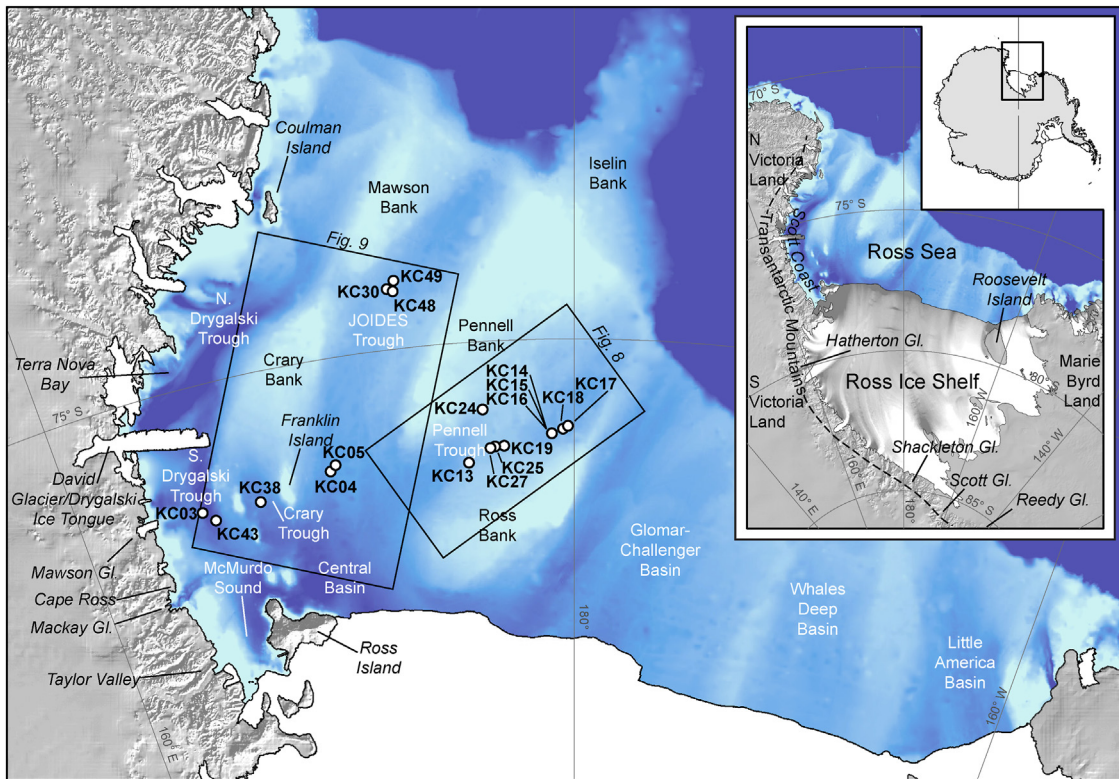


Fig. 1. Map showing location of the Ross Sea Embayment with all mentioned marine and terrestrial locations labeled, as well as core locations for Fig. 6. Black boxes represent locations for Figs. 8 and 9.

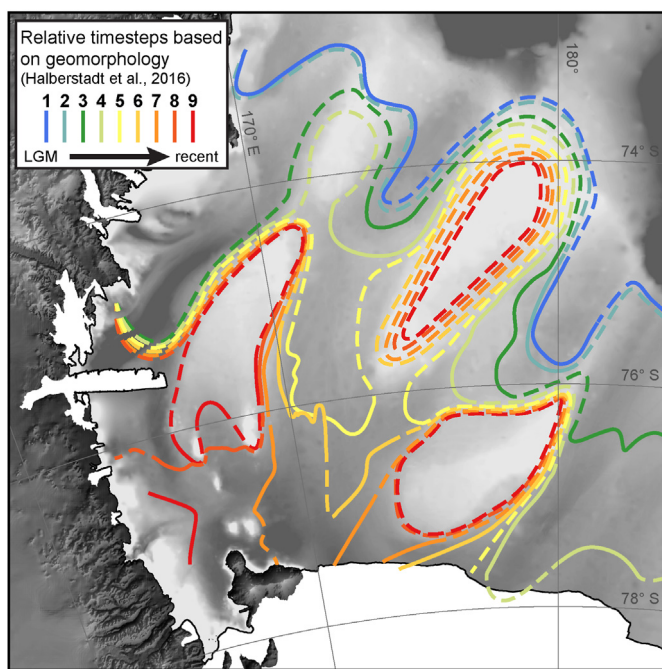


Fig. 2 Reconstruction of grounding-line retreat based on geomorphology as interpreted by Halberstadt et al. (2016). Dashed lines indicate inferred grounding-line position and solid lines indicated geomorphically-constrained grounding-line position. Reconstruction progresses from LGM (blue) to near-present (red). (For interpretation of the references to color in this figure legend, the reader is referred to the Web version of this article.)

Facies 3 (proximal glacimarine basal meltout) is the second type of diamictite recovered along the foresets and toes of grounding-zone wedges, but is characterized by an abundance of soft sediment clasts, or pellets (e.g., Domack et al., 1999; McGlennan et al., 2017; Prothro et al., 2018) believed to be consolidated basal debris that melts out from the ice (Powell et al., 1996; Domack et al., 1999; Cowan et al., 2012; Christianson et al., 2016; Prothro et al., 2018). In the western Ross Sea, this facies appears to be restricted to within 1.5 km of the grounding line (Prothro et al., 2018). Like Facies 2, this facies contains a rich well-preserved assemblage of calcareous benthic foraminifera (Fig. 4; Majewski et al., 2018; Prothro et al., 2018).

Facies 4 (meltwater deposits) is characterized by relatively well-sorted, fine silt deposits with a dominant ~10 µm mode (Domack et al., 1999; McGlennan et al., 2017; Prothro et al., 2018). Placement in stratigraphic successions is random, with deposits of varying thickness being found either above Facies 1, above or within Facies 2 and 3, or in combination with Facies 5. The lack of winnowing in grounding-zone proximal cores and the consistency in grain size across the Ross Sea and in Pine Island Bay (e.g., Witte et al., 2014) leads us to interpret this facies as silt transported via meltwater plumes emanating from the subglacial environment at the grounding line (Prothro et al., 2018). Furthermore, foraminifera assemblages vary from dominance by agglutinated species to calcareous foraminifera, suggesting the presence of this deposit is not dependent on environment, but is likely controlled by an event-based process such as episodic meltwater plumes.

Facies 5 (open marine) is found in core tops and is composed of a diatomaceous sandy silt (Cunningham et al., 1999; Domack et al., 1999; Mosola and Anderson, 2006; McGlennan et al., 2017; Prothro et al., 2018). Its thickness across the Ross Sea appears to be a function of both biogenic productivity and duration of open marine

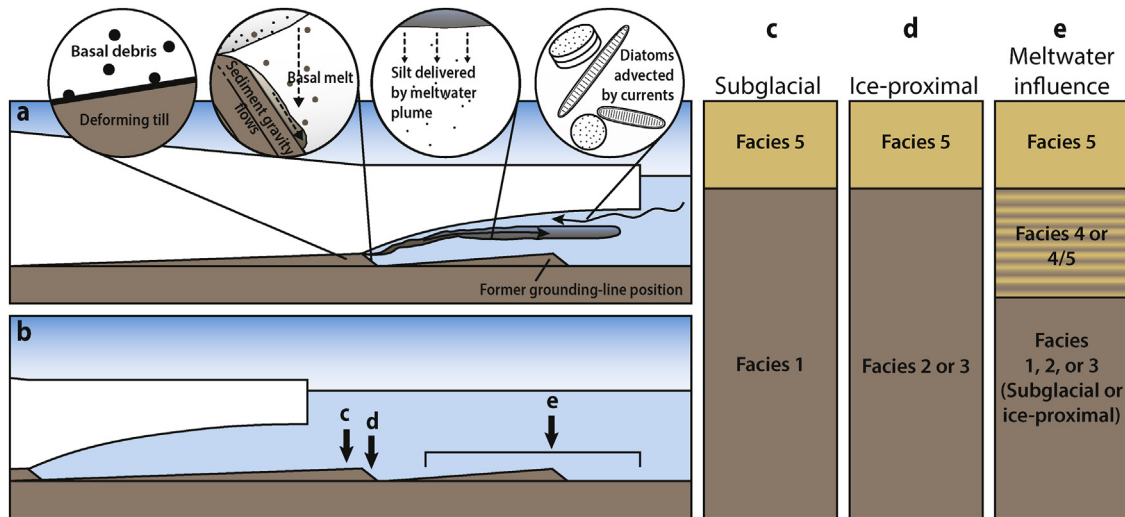


Fig. 3. Conceptual diagram illustrating the formation of different sedimentary facies successions. (a) Timestep 1, demonstrating the processes that occur in the subglacial and proglacial environments to produce stratigraphy, including subglacial deformation of sediments, meltout of basal debris and sediment gravity flows down a grounding-zone wedge foreset, fine sediment expelled in a meltwater plume from the grounding line, and settling of marine detritus from the open ocean, (b) Timestep 2, after the grounding line has retreated (assumes meltwater sedimentation ceased) and open marine conditions prevail. Locations of particular sedimentary successions are denoted by c, d, and e, (c) Sedimentary succession where open marine sediment directly overlies till, with no sub-ice shelf sedimentation (d) Open marine sediments directly overlie proximal glacimarine sediments, with no other sub-ice shelf sedimentation, (e) This location experienced meltwater sedimentation; therefore, whether a core is collected from a subglacial or proglacial environment (Facies 1 vs. 2 or 3), meltwater silt (Facies 4) or some combination of facies is deposited prior to the establishment of open marine conditions.

conditions (Dunbar et al., 1985; Smith et al., 2003; Prothro et al., 2018). Grain size distributions of Facies 5 are fine-skewed with a coarse silt mode or are bimodal with an additional mode at ~10 µm (McGlannan et al., 2017; Prothro et al., 2018), representations of diatom accumulation and meltwater plume sedimentation, respectively (Prothro et al., 2018). Foraminifera are predominantly agglutinated and clearly reworked specimens are not present (Fig. 4; Prothro et al., 2018).

Facies 6 (residual glacimarine) is composed of poorly sorted muddy sand and gravel. Strong coarse skewness reflects winnowing of finer material (Anderson, 1999). This facies is confined to the continental shelf margin, upper continental slope, and bank tops, where relatively strong bottom currents are known to occur (Jacobs et al., 1974; Anderson, 1999). Given its reworked nature, foraminiferal analysis was not conducted on this facies, although residual glacimarine sediments from other parts of the Antarctic margin contain reworked assemblages (Milam and Anderson, 1981).

2.2. Dating deglacial sediments

The onset of open marine productivity, particularly of siliceous organisms, results in an influx of organic detritus to the seafloor that is highly corrosive to calcareous organisms, resulting in poor preservation of carbonate material that would otherwise be used for dating (Kennett, 1968; Milam and Anderson, 1981). Thus, there has been a strong reliance on using acid-insoluble organic (AIO) material from bulk sediment samples. AIO is advantageous because it does not require large sample sizes and the measurement is relatively quick. Although it is meant to measure syndepositional organic matter, there is no way for AIO to exclude any reworked carbon delivered by glaciers or icebergs. Examples of bias in ages obtained from AIO compared to more reliable methods have been shown across Antarctica, in the Ross Sea (Yokoyama et al., 2016a), the Antarctic Peninsula (Rosenheim et al., 2008, 2013; Mackintosh et al., 2011; Subt et al., 2016; Minzoni et al., 2017), and East Antarctica (Leventer et al., 2006).

Compound-specific radiocarbon dating offers a solution to contamination of samples by relict carbon. First introduced by Eglington et al. (1996), the compound-specific method measures the

carbon isotopic composition ($\delta^{13}\text{C}$ and radiocarbon) of individual organic compounds. The greatest challenge for compound-specific dating lies in obtaining adequate quantities of sample to extract enough datable compounds (Ingalls and Pearson, 2005). Sample sizes required for dating are dependent upon sedimentary facies. Although uncertainties may be large for compound-specific ages (Yamane et al., 2014; Yokoyama et al., 2016a), the entire range of uncorrected ages recovered through compound-specific methods are clearly younger than uncorrected AIO ages (Yokoyama et al., 2016a).

In paleo-ice-proximal environments of the western and central Ross Sea that were protected from corrosive organic material by a floating ice shelf, carbonate material has been relatively well-preserved (Bart and Cone, 2012; Prothro et al., 2018). Despite this advantage, dating calcareous material is still problematic because populations of calcareous organisms living in ice-proximal settings are subjected to reworking by fluctuating ice and mixing by sediment gravity flows (Bart and Cone, 2012) and can produce suspiciously old ages (Bart et al., 2016). However, with careful consideration of test condition (i.e. unbroken with no signs of discoloration, physical damage, or chemical dissolution) combined with investigation of foraminiferal assemblages, in-situ foraminifera can be identified and used for obtaining accurate constraints on grounding-line retreat (e.g., Bart et al., 2018).

Geomorphic context becomes incredibly important for distinguishing facies that yield useful ages (such as some ice-proximal sediments) from facies that provide little to no valuable age information about grounding-line retreat (such as till). As shown in Fig. 3, formerly subglacial locations such as fields of glacial lineations and topsets of grounding-zone wedges commonly record sedimentary successions with till (Facies 1) overlain by open marine deposits (Facies 5). Stratigraphy-forming volumes of distal sub-ice shelf deposits derived from meltwater are rare due to limited and intermittent meltwater production (Prothro et al., 2018); thus, the boundary between the till (Facies 1) and the open marine facies (Facies 5) may be a hiatus of unknown duration. Therefore, although an AIO or compound-specific age obtained from just above this boundary can be confidently interpreted as the age of ice shelf loss, it can only be considered a minimum age of grounding-

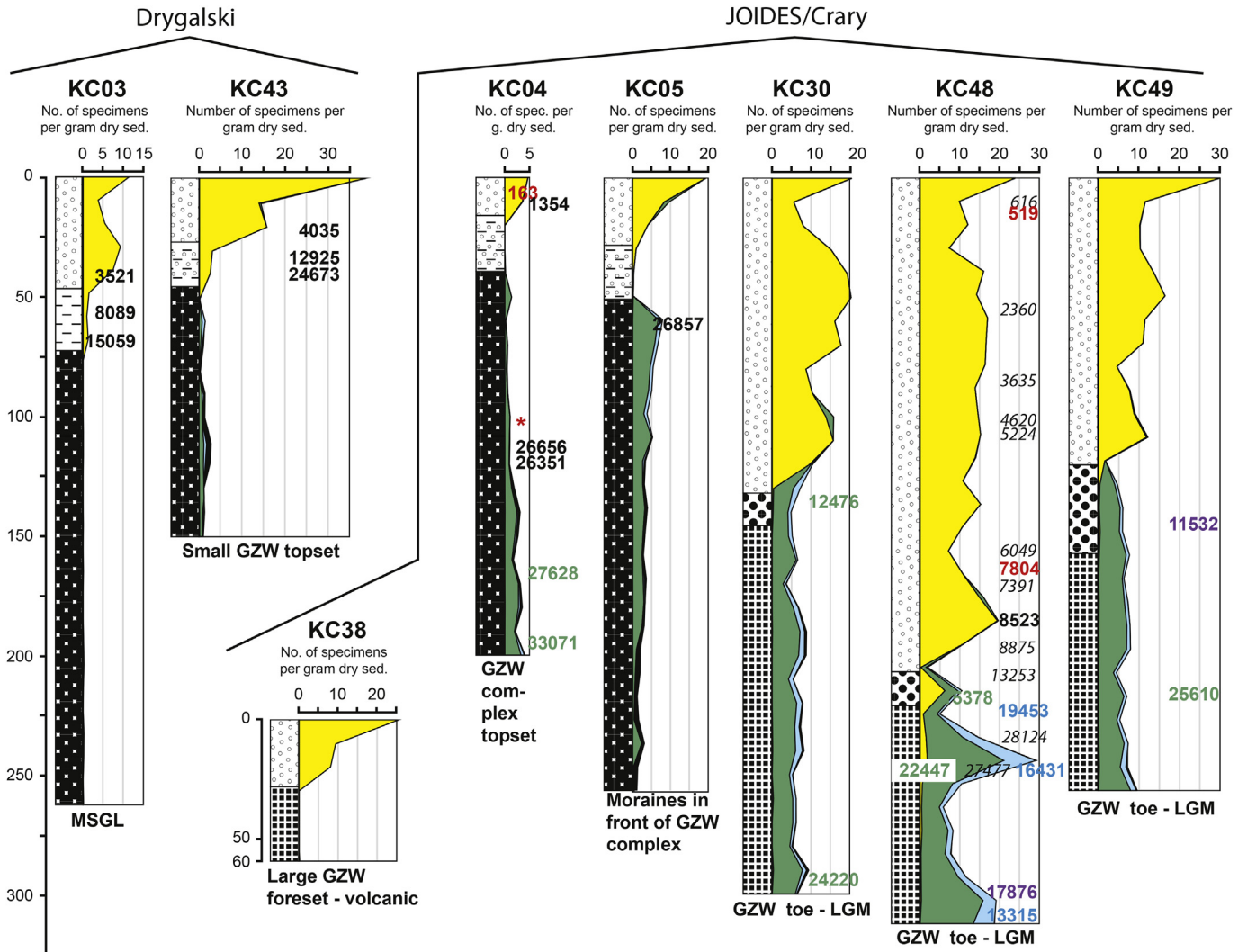


Fig. 4. Downcore foraminifera composition, habitat, and preservation data for key cores in JOIDES and Pennell troughs. Facies are denoted according to Prothro et al. (2018) nomenclature: 1 – Till, 2 – Proximal glacimarine debris flows, 3 – Proximal glacimarine basal meltout, 4 – Meltwater deposit, 5 – Open marine. Calibrated radiocarbon ages are displayed on downcore logs and classified according to key. Italicized ages on KC48 are pulled from NBP9501 KC39. Details of radiocarbon ages can be found in Table C1 (supplementary data).

line retreat. Cores from ice-proximal settings (grounding-zone wedge foresets and toes) are better positioned for determining grounding-line retreat timing, containing successions of grounding-zone proximal sediments (Facies 2 or 3) overlain by open marine deposits (Facies 5; Prothro et al., 2018). Ross Sea grounding-line retreat chronologies have often been constructed using AIO radiocarbon dating of the sediments directly above the transition from subglacial or sub-ice shelf facies to Facies 5 (e.g., Licht et al., 1996), but Bart and Cone (2012) were among the first to recognize that this method might result in significant underestimation of timing of ice sheet retreat, as this transition is only a representation of the removal of some type of ice cover (i.e., ice sheet, ice shelf, permanent sea ice). The strategy of taking the youngest carbonate age from a diamicton at a grounding-zone wedge foreset to represent the maximum age of the grounding event (Licht and Andrews, 2002) is likely a better practice.

2.3. Marine records of retreat

Previous assessments of Ross Sea Late Quaternary glacial history generally place initial post-LGM retreat of the EAIS after 13 cal ka BP

with rapid retreat during the Holocene (Domack et al., 1999; Anderson et al., 2014). These assessments are based on acid insoluble organic (AIO) dating of glacimarine sediments in cores collected just north of the inferred (from Licht et al., 1996) LGM grounding line in JOIDES Trough (Fig. 1; Cunningham et al., 1999; Domack et al., 1999). Existing data regarding timing of grounding line retreat in individual troughs are sparse. Timing of initial grounding line retreat in the westernmost trough (Drygalski) is poorly-constrained but the maximum extent of the grounding line is inferred from a large grounding-zone wedge just north of Coulman Island (Shipp et al., 1999; Halberstadt et al., 2016). Licht et al. (1996) report outer continental shelf AIO ages ranging from 20 to 29 cal ka BP in glacimarine sediments; this, coupled with sedimentological evidence of tephra layers, suggests that the ice sheet did not advance far past Coulman Island prior to and during the LGM. This is consistent with the occurrence of bioclastic carbonates on the outer portion of Mawson Bank that have yielded LGM ages (Taviani et al., 1993). By ~11 cal ka BP, the grounding line in Drygalski Trough is thought to have retreated to the vicinity of the modern Drygalski Ice Tongue (Licht et al., 1996; Cunningham et al., 1999; Domack et al., 1999), but a floating ice shelf appears to have

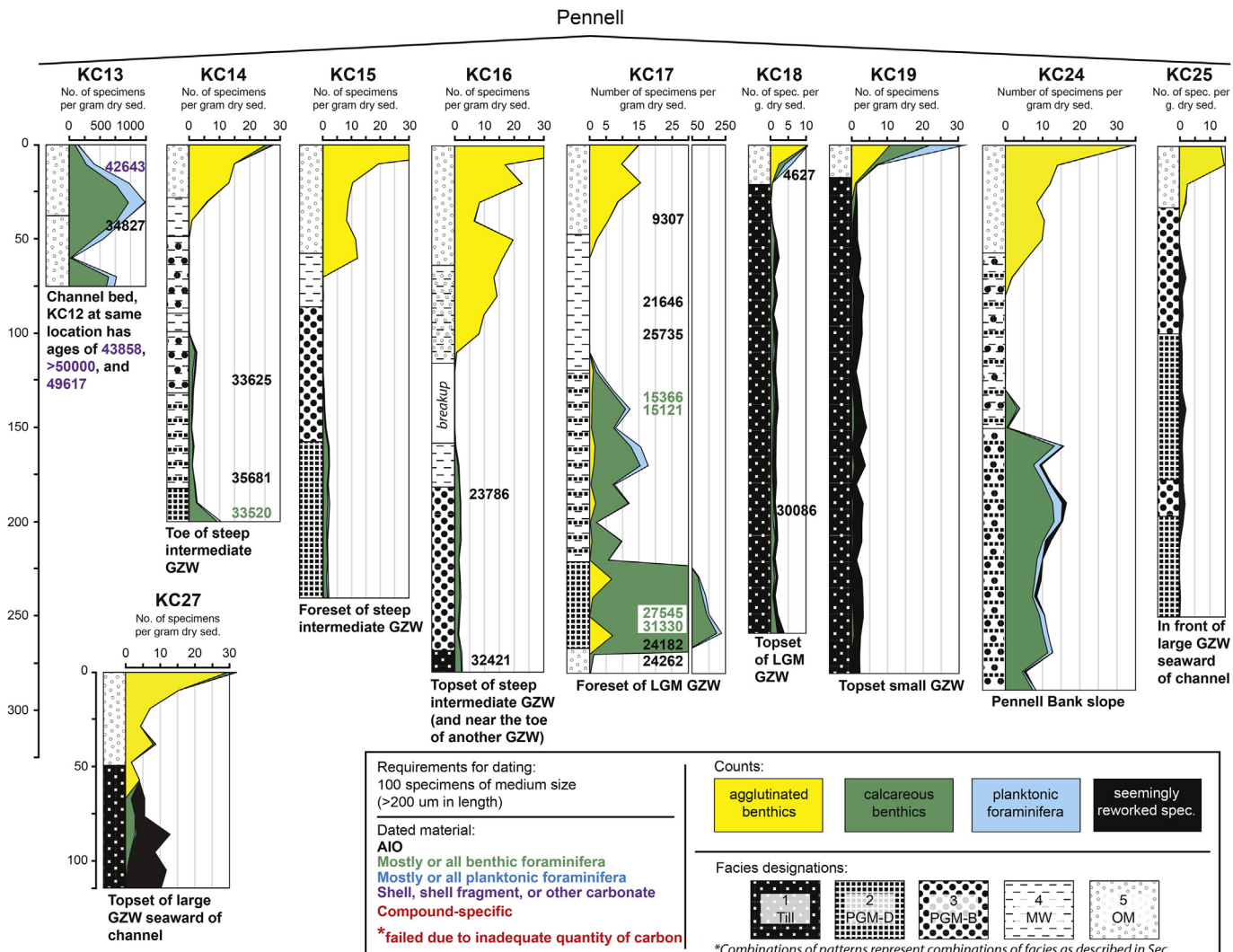


Fig. 4. (continued).

persisted as far north as Terra Nova Bay until ~8 cal ka BP (Yokoyama et al., 2016a). While the ice shelf remained widespread, the grounding line appears to have rapidly retreated southward to the vicinity of Ross Island by 8.6 cal ka BP (McKay et al., 2016) and to the south of Ross Island by ~7.8 cal ka BP (Licht et al., 1996; McKay et al., 2008, 2016). McKay et al. (2016) suggested that the observed increase in diatoms and coarse sediment at the Ross Island-adjacent sites indicates a short period of open water closely associated with grounding line retreat, but noted that advection beneath an ice shelf could possibly be responsible for the this facies change. The aforementioned 13 cal ka BP grounding line retreat in JOIDES Trough (Domack et al., 1999; Anderson et al., 2014) is supported by a single radiocarbon age from carbonate material that places grounding line retreat sometime after ~18 cal ka BP (Yokoyama et al., 2016a). Based on ages from the onset of diatomaceous sediment accumulation, the outer continental shelf of JOIDES Trough was reported to have been fully marine by ~11 cal ka BP (Cunningham et al., 1999; Domack et al., 1999). Pennell Trough, to the east, has been sparsely studied. A single core from the flank of Pennell Bank was used to suggest grounding line retreat occurred at ~13.3 cal ka BP (Domack et al., 1999), but this AIO age has since been refined on the basis of a compound specific radiocarbon age at the same location and depth of ~5 cal ka BP (Yokoyama et al., 2016a). However, this late Holocene age is not necessarily reflective of

grounding line retreat in Pennell Trough but rather the collapse of a bank-pinned ice shelf that occurred across much of the western Ross Sea at this time (Yokoyama et al., 2016a).

Recent analyses of retreat paths based on mapping of glacial lineations and grounding-line landforms such as moraines and grounding-zone wedges suggest retreat in the western Ross Sea was complex, with ice streams retreating from deep within troughs up onto banks, at times from south to north (Halberstadt et al., 2016; Lee et al., 2017; Simkins et al., 2017; Greenwood et al., 2018). The opening of a grounding line embayment in the central Ross Sea (Ackert, 2008; Golledge et al., 2012; Halberstadt et al., 2016) may have enabled an ice flow direction change in the western Ross Sea and triggered enhanced flow and associated ice sheet readvance from outlet glaciers along the South Victoria Land Transantarctic Mountains (TAMs; Greenwood et al., 2018). Preexisting simple north to south retreat scenarios and regional generalizations (e.g. Conway et al., 1999) are considered inadequate for describing the evidently complex ice sheet retreat history of the Ross Sea as observed in the offshore bathymetry (Halberstadt et al., 2016).

2.4. Terrestrial records of retreat

Lag times between marine grounding-line retreat and upstream

(terrestrial) thinning are unknown, at present constrained only by modelling studies (Anderson et al., 2004; Payne et al., 2004; Favier et al., 2014; Joughin et al., 2014) rather than observational data. Still, the history of ice sheet thinning on the terrestrial margin of the Ross Sea is well-studied and is essential for understanding feedbacks between the marine and terrestrial records of ice-sheet behavior. The most widely cited terrestrial reconstruction of post-LGM Ross Sea deglaciation describes the retreating ice as a “swinging gate” hinged on a pinning point created by Roosevelt Island and rapidly opening southward along the TAMs (Stuiver et al., 1981; Conway et al., 1999). Previous and subsequent terrestrial studies do not strongly deviate from this model, but rather have added better constraints on rates of retreat southward along the Transantarctic Mountains (e.g. Hall et al., 2004, 2013). The “swinging gate” model was originally based only on data from Roosevelt Island and two locations along the Transantarctic Mountains—Cape Ross (southern Scott Coast) and farther south near Hatherton Glacier (Fig. 1). A later study by Baroni and Hall (2004) contributed the most northern constraint on grounding line retreat past Terra Nova Bay, where organic material from raised beaches gives a grounded ice unloading date of ~8 cal ka BP. Along the southern Scott Coast, similar data suggest the grounding line retreated to the north side of Ross Island by ~7.8 cal ka BP (Hall et al., 2004, 2013). These interpretations are supported by evidence of periods of increased beach formation in southern Victoria Land from 5.0 to 6.0 cal ka BP, 3.0–4.0 cal ka BP, and 0.6–2.0 cal ka BP, which are interpreted to be times when the coast was unshielded from wave energy due to periods of reduced sea ice (Simkins et al., 2015). However, the extrapolation of observations from Roosevelt Island to the TAMs explicitly implies ice streams behaved similarly to each other, which is inconsistent with the marine record.

Farther south at Taylor Valley, near where the modern ice-shelf edge is located in the main Ross Sea Embayment, LGM moraines indicate initial drawdown of ice ranging from 18 to 13 cal ka BP (Hall and Denton, 2000; Hall et al., 2013), and ~16 to 14 cal ka BP near Blue Glacier (Brook et al., 1995; Hall et al., 2013). Locally, grounded ice is reported to have been present in McMurdo Sound from 28.5 to at least 9.0 cal ka BP (Stuiver et al., 1981; Clayton-Greene et al., 1988; Hall and Denton, 2000; Hall et al., 2010a; Hall et al., 2013). Christ and Bierman (2019) report ice at its maximum extent (thickness) in McMurdo Sound until 12.3 cal ka BP, after which it continued to thin. Similarly, at Hatherton Glacier, drawdown of ice began at 13.0 cal ka BP and reached present-day elevations by 6.8 cal ka BP (Bockheim et al., 1989; Hall et al., 2013), and is reported as the southernmost constraint on the original ‘swinging gate’ model (Conway et al., 1999). This age of 6.8 cal ka BP has since been adjusted to 7.9 cal ka BP following the discovery of a modelled 1.1 ky lag between grounding-line retreat of ice in the Ross Sea and upstream thinning for the Hatherton Glacier system (Anderson et al., 2004). Spector et al. (2017) find evidence for subsequent rapid grounding line retreat over ~1 ky from Hatherton Glacier to Shackleton Glacier, followed by slower retreat as Scott Glacier thinned to modern ice elevation over the next ~3 ky. Reedy and Scott glaciers were at their maximum until ~14 cal ka BP, after which thinning has continued (Stone et al., 2009; Todd et al., 2010), but the grounding line has not yet passed Reedy Glacier (Bromley et al., 2012).

3. Materials and methods

3.1. Geophysical data and coring

Data were collected onboard the RV/IB *Nathaniel B. Palmer* during Expedition NBP1502A (Fig. 1) and supplemented by data

from Deep Freeze 80 (DF80), Polar Duke 90 (PD90) and 92 (PD92), NBP9401, NBP9401, NBP9501, NBP9801, NBP9902, and NBP0802. Chirp data were collected using a Knudsen CHIRP 3260 sub-bottom profiler at 3.5 kHz, and bathymetric data were collected using a Kongsberg EM-122 multibeam echosounder. Both chirp and multibeam data were analyzed in real-time to identify ideal geomorphic environments for coring. During NBP1502A, forty-nine sediment cores were collected with Kasten core barrels and two were collected with a jumbo piston corer. Core lengths were sufficient to recover the entire post-LGM sequence as all cores either bottomed out in diamicton or were impeded by a resistant substrate before fully filling the barrel. Once onboard, Kasten cores were cleaned, photographed, and visually described before sampling onboard. Visual descriptions include Munsell sediment color, texture, sorting, and sedimentary structures. Shear strength was measured at 5–10 cm intervals along each core using a handheld TorVane, and samples for measuring water content and grain size were collected every 5 cm. Approximately 20 cm³ of sediment was collected every 10 cm for analysis of foraminifera assemblages, and preliminary sampling of sediment for radiocarbon analysis at apparent lithologic transitions was performed. Remaining sediment was archived and, following the cruise, was x-rayed and analyzed using a Geotek multi-sensor core logger to recover line-scan images, magnetic susceptibility, p-wave velocity, and gamma-ray derived density. The archived cores are now at the Oregon State University Marine Geological Repository. Legacy cores mentioned in this study are from other expeditions and have not necessarily undergone the same post-acquisition treatment and analyses.

3.2. Sedimentology and micropaleontology

Grain size for NBP1502A cores (Appendix A) was measured using a Malvern Mastersizer Hydro 2000G laser particle size analyzer following treatment with sodium hexametaphosphate to deflocculate grains. Key analyses generated by the Malvern software include grain size mode, cumulative volume percent, and frequency volume percent. Other parameters such as grain size mean, sorting, and skewness were calculated using the methods presented in Folk and Ward (1957).

Sediment samples collected for foraminiferal analysis were wet-sieved through 63 µm and 125 µm sieves and dried. Foraminifera in the finer fraction (63–125 µm) are highly diluted with respect to terrigenous sediment, so the >125 fraction was picked exclusively. For samples with abundant foraminifera, a micro-splitter was used to divide dried samples before picking. Only specimens exhibiting translucent, non-etched tests were classified and quantified as potentially *in-situ* or syndepositional. These foraminifera were sorted into 40 species and grouped into agglutinated and calcareous benthics as well as planktonics, all presented in this study as abundances per gram of dry sediment (Fig. 4). Each data point represents a volume of approximately 20 cm³ (dry weight range ~10–50 g) spanning 2 cm of the core length. However, at these volumes, few cores contain adequate numbers of foraminifera for dating in a single sample. Much larger volumes were required for radiocarbon dating foraminifera in some cores, so successions of two to three samples over 5 or 10 cm of the core length were often combined to obtain a single age. Clearly reworked foraminifera were also counted, identified by signs of abrasion, strong discoloration, or representing species not found in modern Ross Sea sediments. Foraminifera not used for radiocarbon dating are housed at the Institute of Paleobiology of the Polish Academy of Sciences (Warsaw) under the catalog number ZPAL F.71.

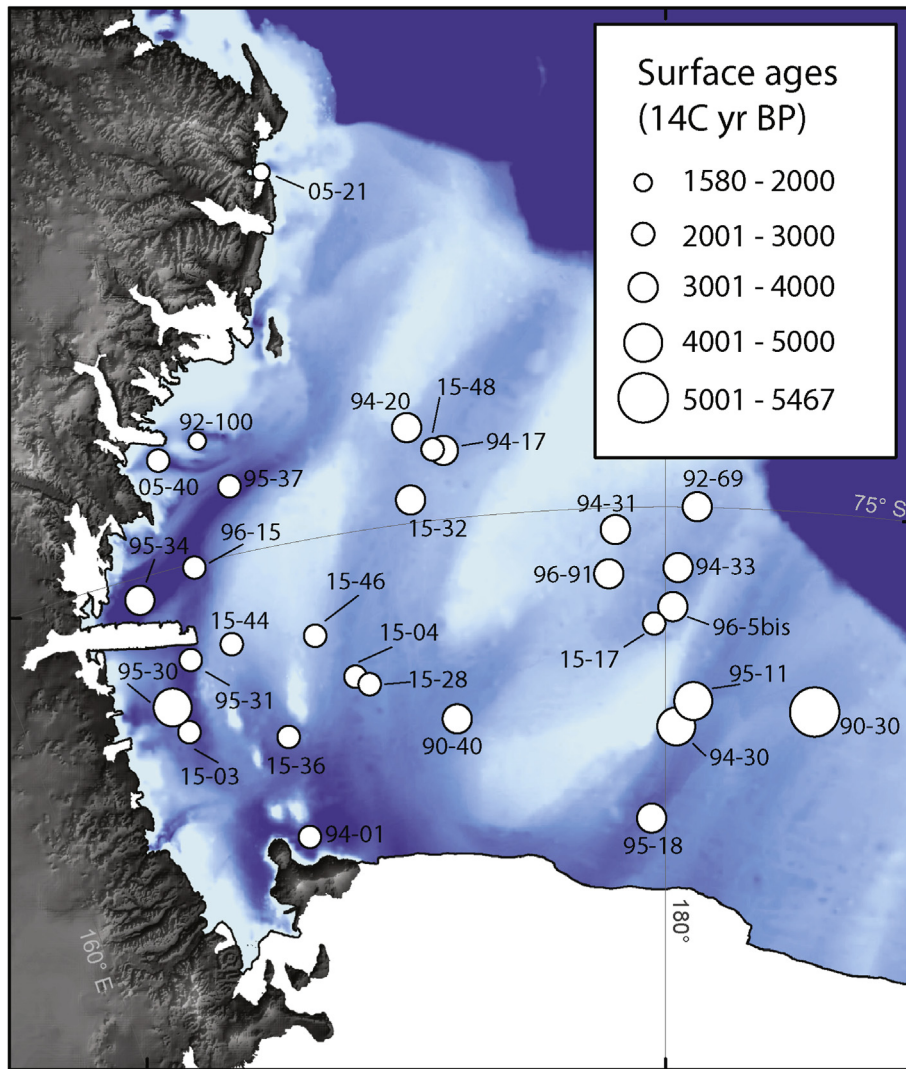


Fig. 5. Distribution of core top (surface) AIO ages. Relative ages are represented by size of core marker. Actual ages are reported in Table 1.

3.3. Radiocarbon dating

We employed three different methods of radiocarbon dating. Analysis of AIO fractions were conducted after samples were oxidized in a glass tube or combusted (at 850 °C) in a specially-designed elemental analyzer and the CO₂ gases were introduced into the vacuum line to convert into the target graphite (Yokoyama et al., 2007). In some horizons with relatively abundant carbonate material, well-preserved foraminifera were picked, sieved, and cleaned ultrasonically before they were treated with a specially-designed vacuum line for small samples (Yokoyama et al. 2010; Hirabayashi et al. 2017). The ages obtained using these methods range widely, with many appearing suspiciously old. Still, by excluding clearly reworked foraminifera (which Fig. 4 shows are present in small quantities in all ice-proximal sediments), we ensure these ages are as reliable as possible. Even so, ages may appear out of order (e.g., KC48, Fig. 4) within ice-proximal sediments and is attributed to mixing by sediment gravity flows. In samples where carbonate material is sparse and recycled carbon is too abundant for accurate AIO fraction ages, we attempted to use compound specific (CS) radiocarbon dating of C₁₄, C₁₆, and C₁₈ fatty acids isolated from the bulk sediment in several cores. Although these compounds are derived from various organisms, they contain

very little relict organic matter due to rapid decomposition (Ohkouchi et al., 2003). Theoretically, CS radiocarbon dating can provide accurate ages that are unaffected by reworked organic material from interior Antarctica. Often, 100–500 g of wet sediment were required to obtain adequate quantities of carbon to conduct the analysis, and only Facies 5 produced sufficient quantities. Detailed descriptions of fatty acid extraction can be found in Ishikawa et al. (2018), and advancements in these methods are provided in Appendix B.

Calibration of ^{14}C ages was performed with Calib 7.0 and the Marine13 calibration curve (Stuiver and Reimer, 1993; Reimer et al., 2013) using a reservoir age of 1300 ± 100 yr (Berkman and Forman, 1996). We apply an additional correction to bring surface ages in each core to zero so we can interpret cores with AIO ages and use the resulting large dataset to help determine the timing of major events. We use the ‘local contamination offset’ (LCO) method, as termed by Hillenbrand et al. (2010), that originated from a widely-used surface correction method (e.g., Domack et al., 1999; Andrews et al., 1999). It is determined from the difference of the surface AIO age of a core (if no such age, take surface age from nearest downstream core) and the Southern Ocean reservoir age of 1300 ± 100 yr. This difference, or LCO, is then subtracted from each AIO age in the core prior to calibration, under the assumption that the organic

Table 1

Surface AIO ages shown in Fig. 2 and used for surface corrections (LCO) before calibrating radiocarbon dates. "Sample depth" refers to the mean of the range of depths used for radiocarbon dating each sample, with 0 always being the upper bound. We have restricted our analysis to mean sample depths of 4 cm or less because earlier studies show a tendency toward analyzing greater volumes of sample, likely resulting in inaccuracies. We also exclude surface ages from cores with a clear concentration in IRD at the surface or that are significantly (>1000 years) older than nearby surface ages, as they are likely biased as well. More details and reasons for exclusion can be found in Appendix C. SD=Standard deviation 1σ. PD=Polar Duke, NBP=Nathaniel B. Palmer. TC=Trigger core, KC=Kasten core, BC=Box core. [Study in which age first reported: 1—DeMaster et al., 1996; 2—Andrews et al., 1999; 3—Cunningham et al., 1999; 4—Domack et al., 1999; 5—Licht and Andrews, 2002; 6—Salvi et al., 2006; 7—Mezgec et al., 2017; 8—this study; 9—Yokoyama et al., 2016a].

Study	Expedition	Core ID	Sample depth (cm)	Water depth (m)	¹⁴ C age (yr BP)	SD (yr)	LCO (yr)	Latitude	Longitude
1	PD90	KC30	3	572	5470	130	4167	-76.488	-175.198
1	PD90	KC40	3	612	3310	90	2013	-76.498	173.328
1	PD92	KC69	3	440	3060	110	1761	-75.000	-179.072
1	PD92	KC100	4	580	1970	95	672	-74.117	167.162
2	NBP9501	KC30	1	752	4350	75	3050	-76.001	164.585
2	NBP9501	KC34	0.5	1257	3210	60	1905	-75.165	164.494
2	NBP9601	BC15	0.5	939	2810	50	1505	-75.033	166.263
2	NBP9601	BC91	0.5	451	3580	50	2280	-75.498	178.328
3	NBP9501	KC31	1	879	2420	50	1124	-75.700	165.418
3	NBP9501	KC37	1	924	2780	50	1480	-74.498	167.743
4	NBP9401	TC1	1	939	2580	55	1280	-77.194	167.888
4	NBP9401	TC17	1	556	3340	45	2040	-74.49	173.801
4	NBP9401	TC20	1	513	3580	50	2280	-74.292	172.863
4	NBP9401	TC30	1.5	628	4620	100	3320	-76.647	-179.636
4	NBP9401	TC31	1	473	3270	50	1970	-75.165	178.548
4	NBP9401	TC33	1	603	3370	50	2070	-75.455	-179.615
4	NBP9501	TC11	1	659	4140	100	2840	-76.453	-179.087
5	NBP9501	TC18	1	819	3740	60	2435	-77.333	179.537
6	ANTA96	5bis	1	568	3820	40	2520	-75.747	-179.759
7	BAY05	BC21	0.5	456	1580	45	280	-72.300	170.050
7	BAY05	BC40	0.5	1033	2230	30	930	-74.183	166.05
8	NBP1502A	KC03	0.5	838	2920	55	1621	-76.216	164.886
8	NBP1502A	KC04	0.5	597	2910	45	1608	-76.078	170.334
8	NBP1502A	KC17	0.5	549	2910	45	1610	-75.874	179.666
8	NBP1502A	KC28	0.5	598	2430	40	1131	-76.147	170.723
8	NBP1502A	KC32	0.5	531	3310	65	2006	-74.829	172.733
8	NBP1502A	KC36	0.5	728	2280	45	979	-76.424	167.895
9	NBP1502A	KC44	0.5	486	2680	45	1384	-75.654	166.808
8	NBP1502A	KC46	0.5	446	2610	45	1311	-75.719	169.336
8	NBP1502A	KC48	0.5	539	2510	60	1209	-74.473	173.511

matter source remains constant downcore. Because piston cores commonly fail to recover surface sediments (e.g. Andrews et al., 1999), we have eliminated all piston core top ages from our analysis (Fig. 5), and only use ages from core types that preserve the sediment-water interface and show no evidence of concentrated ice rafted debris that could contain relict carbon. Because Calib 7.0 includes a default marine reservoir correction of 400 years, we use $\Delta R = 900 \pm 100$ yrs to calibrate all samples—AIO, carbonate, and compound-specific. We report uncalibrated ages in ¹⁴C yr BP or ¹⁴C ka BP and corrected and calibrated ages in cal yr BP or cal ka BP with 1σ error (Table C1).

4. Results

4.1. Variability in surface age of sediments

AIO ages collected from core tops are substantially older than the 1300 ¹⁴C yr reservoir correction in the Ross Sea. Furthermore, surface ages are highly variable across the Ross Sea (Table 1; Fig. 5), suggesting uniform reservoir corrections are insufficient for spatial comparison of ages. Through comparison with compound-specific dates (e.g., KC48; Fig. 6), we demonstrate that AIO ages from organic-rich diatomaceous sediments are generally reliable when a LCO-correction is performed. The variability in surface ages in the Ross Sea (Fig. 5) demonstrates the necessity of performing LCO-correction. The ages in Fig. 5 trend similarly to Andrews et al. (1999) with older surface ages to the north and east. Andrews et al. (1999) recognize the same trend in δ13C values of the bulk organic fraction, which are less depleted in the southwestern Ross

Sea than in other parts. The prevalence across the Ross Sea of older surface ages on the outer continental shelf relative to the inner continental shelf suggests that another process influences the amount of contamination of surface sediments by relict carbon. Relatively strong boundary currents that flow along and onto the continental shelf edge (Jacobs et al., 1974; Pillsbury and Jacobs, 1985) winnow fine sediments and locally produce well-sorted sands with current ripples (Anderson et al., 1984; Dunbar et al., 1985; Anderson, 1999); these surface sediments are thus depleted in organic-rich diatomaceous material. Regardless of the reasons for spatial heterogeneity in AIO surface ages, it is clear that a uniform reservoir correction is insufficient for comparing events in cores across the Ross Sea.

4.2. Radiocarbon constraints on LGM extent

NBP1502A cores from the LGM grounding-zone wedges in JOIDES (KC30, KC48, KC49) and Pennell (KC17) troughs recovered populations of seemingly *in situ* foraminifera from grounding-zone proximal sediments (Facies 2 and 3). However, ages are not typically in stratigraphic order in these facies (Fig. 4). Some benthic foraminifera at the LGM limit in JOIDES Trough are slightly pre-LGM in age (up to 25.6 cal ka BP, KC49, Fig. 4), but most benthic and planktonic foraminifera range from roughly LGM to late Holocene (as young as 11.5 cal ka BP, KC49, Fig. 4) in age. At the Pennell Trough LGM wedge, benthic foraminifera ages in grounding-zone proximal sediments (Facies 2 and 3) range much older, up to 31.3 cal ka BP (KC17, Fig. 4), and the youngest recovered age is 15.1 cal ka BP (KC17, Fig. 4).

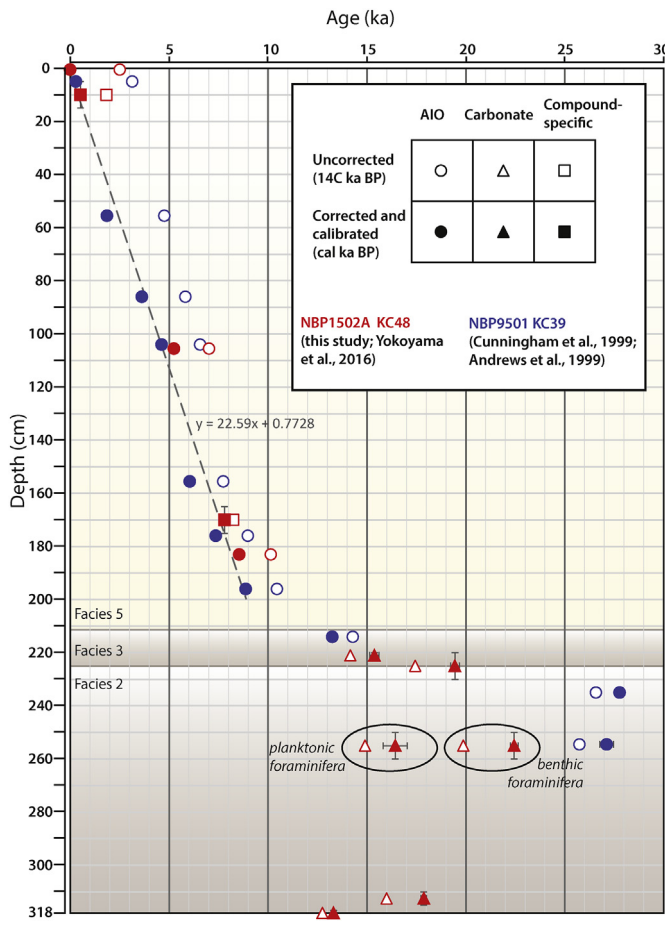


Fig. 6. Downcore plot of uncalibrated and calibrated ages for NBP1502A KC48, demarcated by sedimentary facies. This core is a reoccupation of NBP9501 KC39. Ages for KC39, formerly reported in Cunningham et al. (1999) and Domack et al. (1999) have been incorporated into KC48 at depths selected via lithologic correlation. The surface age for KC48 has been used for corrections rather than the one from KC39.

4.3. Age transitions

We present ages of open-marine onset and grounding-line retreat calculated from new radiocarbon ages as well as those reported in earlier studies of Ross Sea glacial history. Based on multibeam data and core descriptions from publications and cruise reports, we have placed all ages into the context of our facies model from Prothro et al. (2018). We consider most AIO ages from Facies 5 with minimum ice-rafted debris to be viable, given prior mentioned calibrations but we treat AIO ages from subglacial (Facies 1), ice-proximal (Facies 2 or 3) or sub-ice shelf sediments as suspect or invalid in favor of carbonate or compound-specific ages. We recognize a sub-ice shelf facies, hereafter referred to as Facies 4/5, in several Ross Sea cores that shares characteristics with both Facies 4 and 5 (each explained in detail in Section 2.1). These sediments are comprised of relatively well-sorted silts with little to no IRD and often containing fine laminae (like Facies 4), with micro-paleontological characteristics (diatom-bearing, barren or agglutinated-only foraminifera assemblage) of Facies 5. The distinct lack of IRD leads us to interpret these sediments as sub-ice shelf rather than open marine. The combined data are used to calculate or identify the apparent age of ice-shelf loss and grounding-line retreat for each relevant core. Each estimated age of transition is ranked according to reliability based on the criteria described below.

4.3.1. Open-marine onset

The transition from the subglacial (Facies 1) or sub-ice shelf (Facies 4/5) setting to open marine (Fig. 3c, e) is based on a regression calculated from the ages in the open marine facies (c.f. Yokoyama et al., 2016a). We favor this approach over using the youngest age from the underlying facies (e.g., McKay et al., 2008; Bart et al., 2018) because we recognize that even if a sub-ice shelf facies (Facies 4/5) exists below Facies 5, a hiatus in sub-ice shelf sedimentation may exist at the boundary. The age of the transition is calculated at the intercept of the regression curve with the depth of transition as shown in Fig. 6. Ages obtained this way must be from cores with:

- 1) Core descriptions that describe diatomaceous muds
- 2) AIO ages in stratigraphic order
- 3) Minimal IRD content
- 4) Transition depth known

We and others (Yokoyama et al., 2016a; Minzoni et al., 2017) observe AIO ages (LCO-corrected, calibrated, and IRD-free) to be consistent with compound specific ages (e.g., Fig. 6) within open marine sediments (Facies 5); thus, we honor AIO ages within this facies if they meet the other criteria listed above. Ages appearing in stratigraphic order are indicative of minimal vertical mixing from debris flows or extreme bioturbation. Changes in organic matter likely occur downcore (e.g., Domack and Ishman, 1993, Domack et al., 1995; Shevenell et al., 1996; Rosenheim et al., 2008; Michalchuk et al., 2009; Milliken et al., 2009), but the match between AIO and compound-specific ages (e.g., Fig. 6) support the use of LCO-correction in non-IRD-rich open marine sediments (Facies 1). IRD may contain relict carbon, so sandy or pebbly intervals within open marine facies are not be considered in regressions. The depth of transition from the underlying facies to the open marine setting must be clear so the intercept can be calculated. If this depth is unknown (i.e., core does not penetrate far enough), the oldest age in the core is designated as a minimum age of transition. The timing of the open marine transition (ice-shelf or grounded-ice retreat) for individual cores is presented in Table 2, and locations marked in Fig. 7.

4.3.2. Grounding-line retreat

Much of the material deposited in the ice-proximal setting at/near a paleo-grounding line is glacially reworked, having been carried within the basal debris layer of the ice before melting at the grounding line and potentially becoming mixed within debris flows (Domack et al., 1999; Prothro et al., 2018). Thus, the timing of grounding-line retreat is more challenging to determine than that of ice shelf loss. According to Prothro et al. (2018), Facies 2 and 3 are found in association with grounding-zone wedge foresets. Rather than attempting a regression from the age scatter as with Facies 5, the youngest ages acquired from Facies 2 and 3 are most useful for estimating the latest time during which the ice occupied the grounding-zone wedge in question. For cores that lack detailed multiproxy sedimentary analyses from previous studies, geomorphic context is the best indication of ice-proximal facies. For all cores with multibeam data informing facies interpretation, the criteria outlined in Table 3 are considered for ranking grounding-line retreat ages.

Tier 1 ages are those obtained with the best possible dating methods from the grounding-zone proximal environment (Facies 2 or 3) in front of a grounding-zone wedge. This ice-proximal environment also yields unreliable ages when AIO dating is used, so we have excluded these. Unlike the grounding-zone proximal environment, the sub-ice shelf environment is more likely to receive advection of open marine material beneath the ice shelf and be far

Table 2

Calculated ages of open-marine onset and grounding-line retreat. Grounding-line retreat constraints are ranked (Tier 1 is best possible) for viability based on criteria outlined in section 4.3. Open-marine onset ages marked with '(m)' are from cores for which the facies transition was not recovered, so the oldest age in the core is reported here. Grounding-line retreat ages left blank are from cores for which determining the timing of grounding-line retreat was not possible, so the open-marine onset age may be used as a minimum timing of grounding-line retreat. DF—Deep Freeze, NBP—Nathaniel B. Palmer, AN_CH2—ANDRILL Coulman High Site 2. PC—Piston core, TC—Trigger core, KC—Kasten core, GC—Gravity core. [*NBP1502A KC48 is a reoccupation of NBP9501 KC39 core site. Sediment facies and ages are correlated and merged to determine transition ages.]

Cruise	Core	Open-marine onset age	Grounding-line retreat age	Reliability of grounding-line retreat constraint	Latitude	Longitude
Drygalski Trough						
BAY05	GC20c	3479 (m)			-72.300	170.050
ANTA99	GC31	8367			-73.226	170.988
NBP9501	KC37	9734	16,519	Tier 2	-74.498	167.743
TH95	GC1604	9500			-74.549	168.002
BAY05	GC43c	5740 (m)			-74.183	166.050
ANTA91	GC28	9289	13,936	Tier 2	-74.658	167.213
ANTA91	GC29	10,285			-75.183	164.366
DF80	PC102	12,058 (m)			-75.200	163.717
NBP1502A	KC44	6569			-75.654	166.808
NBP9501	KC31	6105	10,574	Tier 2	-75.700	165.417
NBP1502A	KC03	4563	5516	Tier 2	-76.216	164.886
NBP1502A	KC43	4636			-76.319	165.329
NBP9501	PC26	6208 (m)			-76.977	162.890
NBP9501	PC29	3860 (m)			-76.985	162.972
DF80	PC57	7439 (m)			-77.283	165.817
JOIDES Trough						
ANTA99	GC05	14,411			-73.824	175.650
ANTA91	GC14	16,357			-73.874	175.414
NBP1502A	KC49		11,532	Tier 1	-74.373	173.580
NBP9401	TC/PC17	7652			-74.490	173.801
NBP1502A	KC30		12,476	Tier 1	-74.448	173.380
NBP1502A	KC48*	9415	13,315	Tier 1	-74.473	173.511
ANTA91	GC19	7530	12,273	Tier 2	-74.433	173.100
NBP9401	TC20	9957			-74.292	172.863
NBP1502A	KC28	2459	5819	Tier 2	-76.147	170.723
NBP1502A	KC04	1603	4295	Tier 2	-76.078	170.334
NBP1502A	KC46	1677	3576	Tier 2	-75.720	169.336
Pennell Trough						
NBP1502A	KC17	9894	15,121	Tier 1	-75.874	179.666
NBP1502A	KC18	9634			-75.883	179.546
NBP1502A	JPC01	6943	11,186	Tier 2	-76.034	176.820
NBP9401	TC/PC31	5807			-75.165	178.548
NBP1502A	KC22	6107			-75.430	176.196
Central Basin/Crary Trough						
NBP9401	TC/PC01	642 (m)			-77.194	167.888
AN_CH2	GC07		8477	Tier 2	-77.582	171.507
DF80	PC189	6411	7689	Tier 2	-77.200	167.883
NBP1502A	KC36	2500			-76.424	167.895
NBP1502A	KC41	2005			-76.405	167.538
Central Ross Sea						
NBP9501	TC/PC11	6981			-76.453	-179.087

enough from the grounding line to not be biased by reworked carbon. Tier 2 is designated to the sub-ice shelf facies (Facies 4/5 combination; see section 4.1.6), which represents sediment deposited after the grounding line has retreated. Except for the timing of grounding line retreat based on a sub-ice shelf (Facies 4/5) carbonate age reported by McKay et al. (AN-CH2: GC07; 2016), these ages are selected by taking the age at which a regression from the core top intercepts the base of the sub-ice shelf facies. Tier 2 regressions exclude all sub-ice shelf AIO ages to reduce bias from reworked carbon; thus, regressions are extrapolated from the open marine facies (Facies 5), above. Ages from Facies 4/5 should be taken as minimum constraints on grounding line retreat because deposition in the sub-ice shelf environment may not occur immediately following grounding-line retreat (Kellogg and Kellogg, 1986, 1988). Instead, deposition is dependent on delivery by meltwater plumes and marine currents, which may be inconsistent (Fig. 3c). For cores for which we are unable to determine the timing of grounding line retreat but ice shelf retreat is known, we take the timing of ice shelf loss as a minimum age of grounding line retreat. All interpreted transition ages are presented in Table 2, and

locations are shown in Fig. 7.

5. Discussion

5.1. Age of the LGM

Carbonate ages from seemingly *in-situ* foraminifera at the LGM limit in JOIDES Trough extend back to 25.6 cal ka BP (KC49, Fig. 4), and to 31.3 cal ka BP (KC17, Fig. 4) in Pennell Trough. In JOIDES Trough, this foraminifera age, along with the timing of grounding-line retreat (KC49, Table 2), bracket the LGM maximum extent to 25.6–11.5 cal ka BP. However, Pennell Trough foraminifera ages from locations seaward of a large subglacial channel (Fig. 8c) may be suspect. Two cores (KC12 and KC13) collected from the channel bed indicate that the channel eroded through LGM till into pre-LGM open marine sediments. Carbonate ages from foraminifera and an intact bryozoan from these sediments (Facies 5) range from 42.6 cal yr BP (KC13) to radiocarbon-dead (KC12, Fig. 4). We suspect that when the channel was active during the LGM and subsequent grounding-line retreat, older eroded channel bed material may

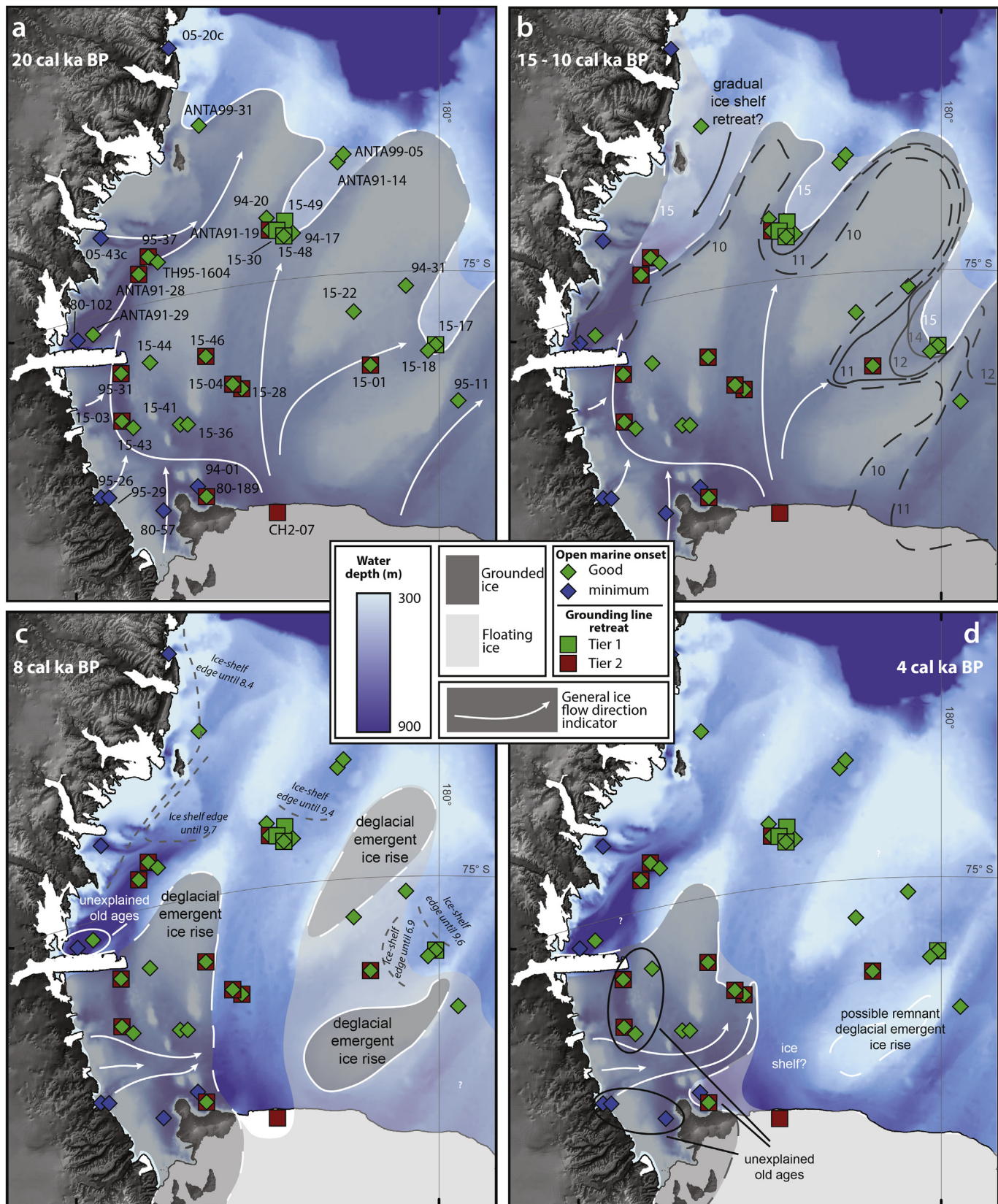


Fig. 7. Reconstructions of grounding line and ice shelf position are based on transitions identified in Table 2 and Fig. C1 (supplementary data). Grounding-line locations based on geomorphic indicators and age control are marked with solid lines and grounding-line locations based on inferences are dashed. Subtle grounding line changes from 14 to 11 cal ka BP marked with grey lines overlie the 15 cal ka BP ice sheet configuration shown on panel 7b—combined for brevity.

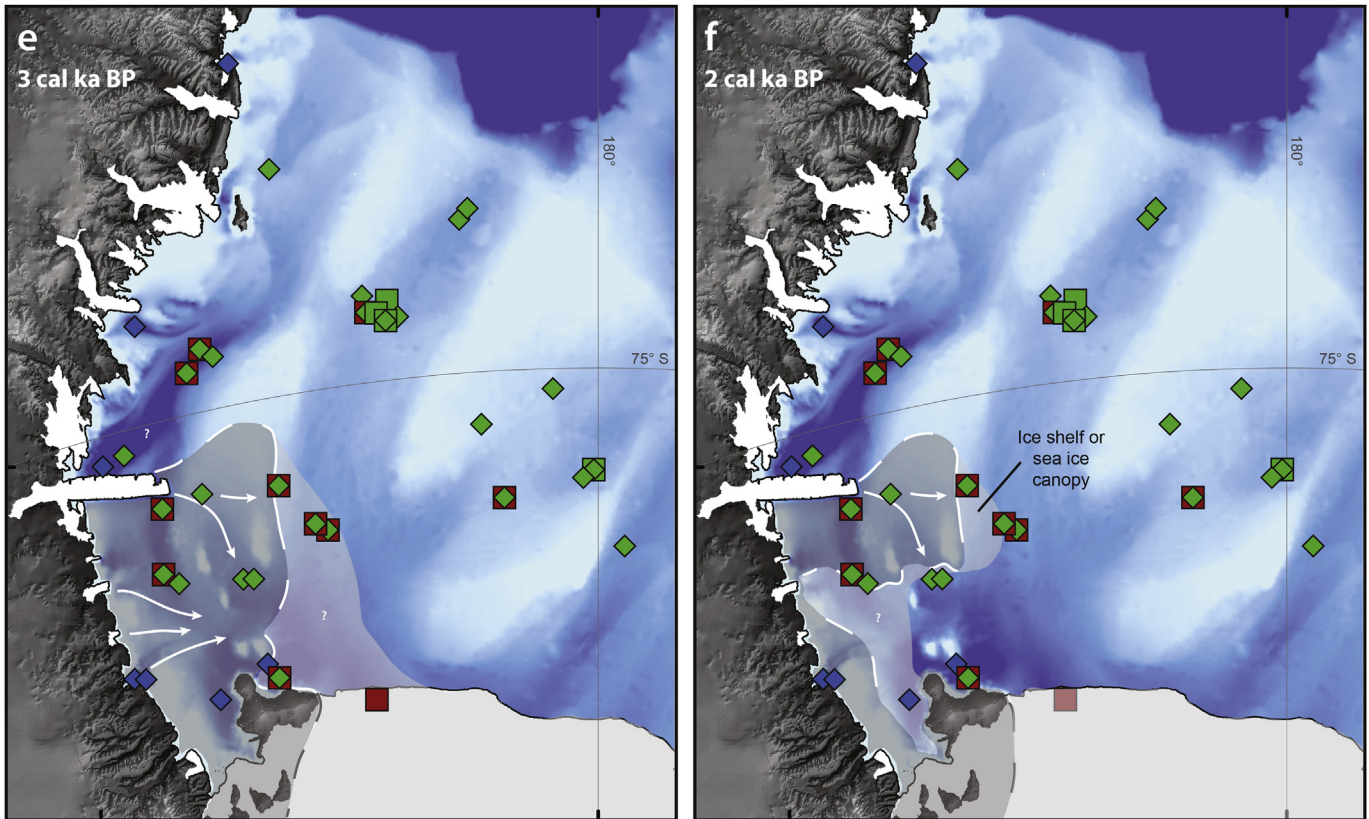


Fig. 7. (continued).

have been transported through it to be deposited at the grounding line, possibly biasing any ages collected there within ice-proximal sediments. This could explain why the AIO ages taken at the base of the core (KC17, Fig. 4) from the pre-LGM open marine unit (Facies 5) over which Facies 2 downlaps (Fig. 8b) are younger than the foraminifera ages above. Using the AIO ages from the lower Facies 5 in KC17 to bracket the upper bound of the grounding-line's LGM limit, and grounding line-retreat age (Table 2) as the lower bound, we can estimate that the ice was at its maximum extent from approximately 24.2–15.1 cal ka BP.

The timing of initial grounding-line retreat in the western Ross Sea is somewhat concurrent with that of ice in Whales Deep in the eastern Ross Sea, which Bart et al. (2018) show began retreating sometime before 14 cal ka BP. There, the WAIS remained near the continental shelf edge until at least 11.5 cal ka BP, after which a ~200 km retreat commenced. This major retreat episode could be contemporaneous with the retreat of the EAIS from the outer continental shelf across much of the western Ross Sea (Fig. 7c and

Yokoyama et al., 2016a). However, there is no evidence from the Ross Sea sector that either ice sheet was a significant contributor to Meltwater Pulse 1A (MWP 1a). During MWP 1a, retreat of both the WAIS and EAIS was minimal and large-scale ice-shelf collapse and grounding-line retreat did not occur until later. The ages presented here for EAIS grounding line retreat do, however, indicate eustatic sea level contributions from the EAIS well through the middle Holocene.

5.2. Deglacial history (LGM – 4 cal ka BP)

We present a reconstruction of western Ross Sea ice sheet and ice shelf retreat since the LGM (Fig. 7), using the calculated ages in Table 2 to estimate the approximate position of the grounding line and the open marine transition at each time step. Due to our local, core-specific corrections and calibrations, we observe somewhat different timing than has previously been published.

Interpreting grounding line behavior requires consideration of

Table 3

Facies designations for all cores listed here are supported by both sedimentological and micropaleontological observations. Ideally, for Tier 1, the youngest age is selected from a sample size of two or more within a facies to represent the timing of grounding-line retreat. For Tier 2, we perform a regression based on ages from the core surface to the transition between Facies 4/5 and Facies 2 or 3. Ages determined this way are not particularly reliable due to possible relict carbon and inconsistent sedimentation rates in Facies 4/5. [*Age is based on single carbonate age, but correlates with ages from equivalent facies in KC48 from the same grounding-zone wedge.]

	Tier 1	Tier 2
Facies	Grounding-zone proximal (Facies 2 or 3)	Sub ice-shelf (Facies 4/5)
Material dated	Carbonate or compound-specific	Carbonate, compound-specific, or AIO
Sample selection	Youngest of two or more	Regression extrapolated from open marine (exception AN-CH2 GC07, single age)
Cores	NBP9902: TC07 NBP1502A: KC17, KC30*, KC48 (same location as NBP9501 KC39), KC49*	NBP1502A: JPC01, KC03, KC04, KC28 DF80: PC189 NBP9501: KC31 AN-CH2: GC07

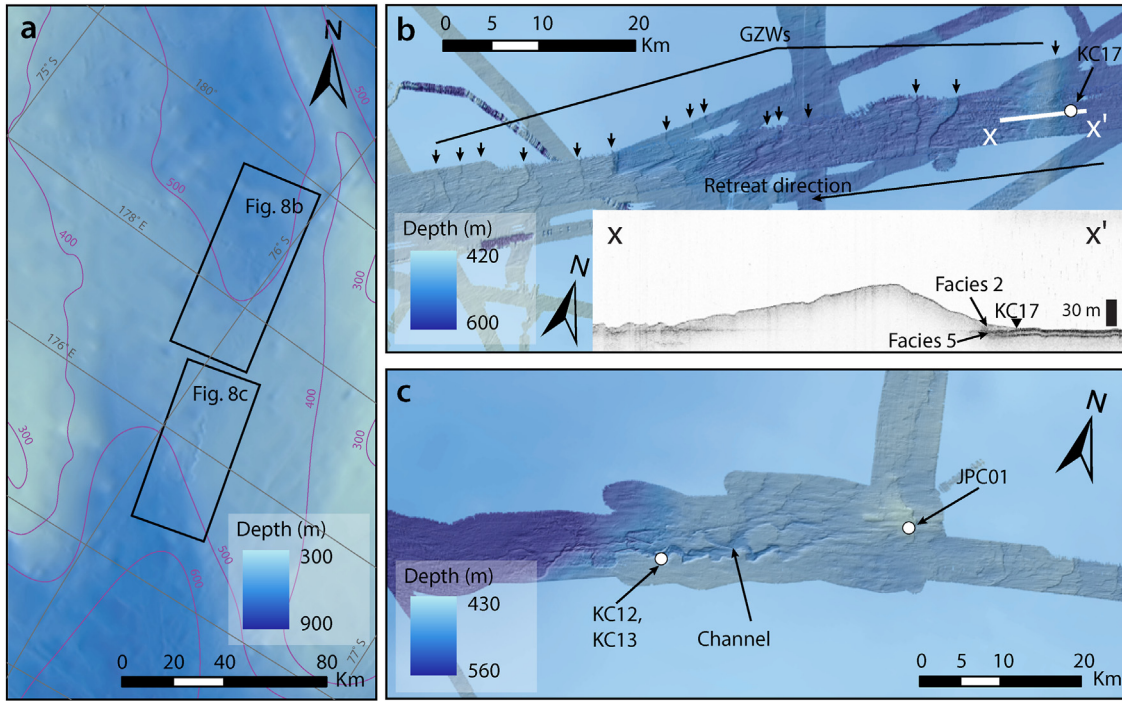


Fig. 8. Pennell Trough geomorphology (a) Overview of the locations of key geomorphic features in Pennell Trough with 100 m depth contours, (b) Continuously backstepping GZWs from the LGM GZW to the bathymetric saddle. Inset depicts x–x' CHIRP profile across the LGM GZW with location of NBP1502 KC17 marked and general facies labeled, (c) Large subglacial channel in Pennell Trough that eroded into pre-LGM sediments.

geomorphic indicators of ice flow direction and retreat patterns in addition to reliable radiocarbon age data. Our data show strong agreement between geomorphic patterns of retreat (e.g., Halberstadt et al., 2016) and radiocarbon ages on the outer continental shelf of JOIDES and Pennell Troughs. The grounding line did not reach the continental shelf edge during the LGM in either trough, but instead was located on the mid-outer shelf (Fig. 7). In Pennell Trough (Figs. 1 and 8), the grounding line appears to have first retreated from the LGM limit at 15.1 cal ka BP (KC17, Table 2) and gradually pulled back to a mid-shelf bathymetric saddle (Fig. 8a) by 11.2 cal ka BP (JPC01, Table 2). Gradual, or episodic, retreat is indicated by grounding-zone wedges that backstep along the trough axis (Fig. 8b) and up the flanks of the banks (Halberstadt et al., 2016) to form a grounding-line embayment akin to a calving bay (Domack et al., 2006; Hogan et al., 2016). Geomorphic observations are supported by ice shelf retreat ages that demonstrate a ~3 ky lag in onset of open marine conditions between the trough axis (KC17, KC18, JPC01, Table 2) and Pennell Bank (KC22 and TC/PC31, Table 2). By taking the ice shelf retreat ages on Pennell Bank as estimates of grounding-line retreat as well, we suggest that grounded ice persisted 5–7 ky longer on Pennell Bank than in outer Pennell Trough. We interpret this configuration of grounded ice on banks surrounded by an ice shelf to be consistent with the ‘deglacial emergent’ style ice rise of Matsuoka et al. (2015). In this scenario, semi-independent ice rises pinned on shallow banks are simply remnants of once-thicker ice and are not indicative of active streaming.

JOIDES Trough (Figs. 1 and 9) appears to have first experienced grounded ice retreat from the LGM limit at ~13 cal ka BP (KC48, Table 2). Open marine onset ages at the LGM limit cluster around 7.5 and 9.5 cal ka BP. We interpret 9.4 cal ka BP (KC48, Table 2) as the true onset of open marine conditions, and the ~7.5 cal ka BP event in some cores to represent the timing of iceberg scouring at those locations. Much of the middle continental shelf in JOIDES

Trough is covered by deep, linear iceberg furrows (Fig. 9b) suggesting that sometime following 9.4 cal ka BP, the Ross Ice Shelf collapsed all the way back to the grounding line to form an ice cliff (Yokoyama et al., 2016a). Further south, small, regularly-spaced grounding-line landforms backstep for 80 km (Fig. 9c and d) but are overrun by a ~20-m high grounding-zone wedge complex (Fig. 9d) that represents a major readvance of a lobe of the EAIS following a reorganization of ice flow in Drygalski Trough (Greenwood et al., 2018).

North of the Drygalski Ice Tongue, N–S oriented glacial lineations overprinted by grounding-zone wedges backstep southward and then toward the Transantarctic Mountains indicate ice from Transantarctic glaciers initially flowed north (Greenwood et al., 2018). The timing of retreat in northern Drygalski Trough is uncertain. We report two Tier 2 grounding-line retreat ages of ~16.5 cal ka BP and ~13.9 cal ka BP (KC37 and GC28, Table 2) in northern Drygalski Trough but are skeptical of their validity for the reasons outlined in Section 4.3.2. However, the ~9.5 cal ka BP open marine onset age for cores in that area (KC37, GC1604, GC28, Table 2) is believed to be accurate, and could be interpreted as a minimum age of grounding-line retreat for the Terra Nova Bay region. However, open marine ages (from PC102 and GC29) to the south of the ~9.5 cal ka BP cluster are older than those to the north, calling into question their validity, especially because we see no geomorphic evidence that the locations of these two cores deglaciated prior to KC37, GC1604, and GC28.

Following the retreat of northern Drygalski Trough, ice in southern Drygalski Trough switched to flow southward (Lee et al., 2017; Greenwood et al., 2018) and eastward around Crary Bank into mid-JOIDES Trough where the grounding line location is marked by an intermediate-sized (Halberstadt et al., 2016) composite grounding-zone wedge (Fig. 9d). This wedge overprints moraines for at least 50 km to the south (Greenwood et al., 2018), indicating that the wedge represents a readvance of ice after a

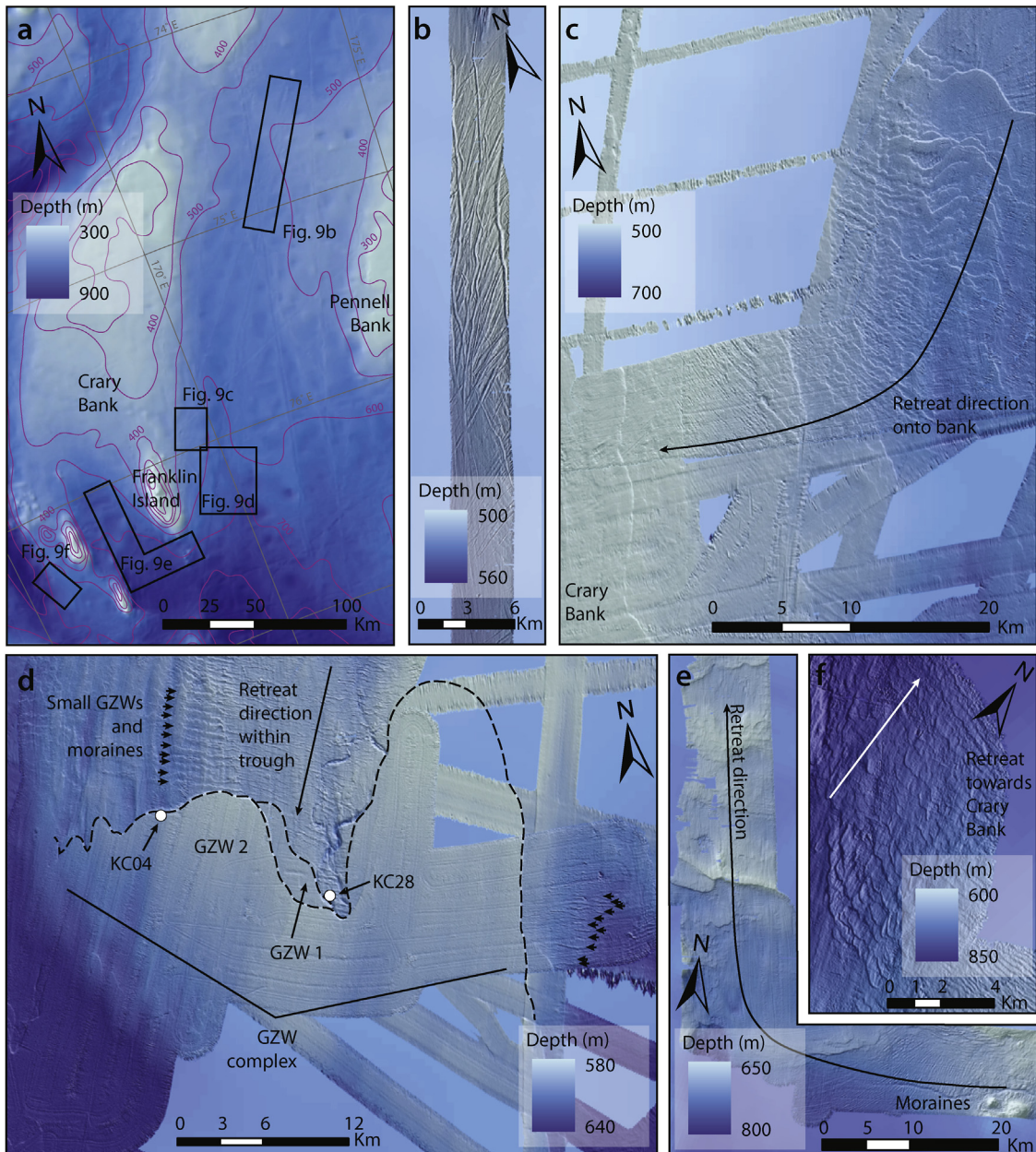


Fig. 9. JOIDES Trough geomorphology (a) Overview of the locations of key geomorphic features in JOIDES Trough with 100 m depth contours, (b) A segment of the field of linear furrows that covers the middle and outer portion of the trough, (c) Grounding-zone wedges (GZW) indicate a change in retreat direction, from south-southwest retreat to westward retreat up onto Crary Bank, (d) Small GZW and moraines indicate a southward retreat direction prior to the readvance of a GZW complex that progrades over the small landforms, (e) Recessional features indicate westward retreat past the southern edge of Franklin Island followed by northward retreat up onto Crary Bank, (f) Small grounding-line landforms indicate eastward retreat from Drygalski Trough onto Crary Bank.

significant retreat of the grounding line (associated with the ice shelf collapse indicated by the iceberg furrows in Fig. 9b). Ice may even have retreated as far as the ANDRILL Coulman High site (McKay et al., 2016), where a foraminifera age from a single core at (CH2-07, Table 2) has been used to suggest an early episode of open water at 8.6 cal ka BP (recalibrated to 8.5 cal ka BP in this paper) with grounding-line retreat even earlier (McKay et al., 2016). As we have discussed, foraminifera ages in the Ross Sea should be treated with caution if collected from sub-ice shelf or ice-proximal sediments. However, the ages presented by McKay et al. (2016) were paired benthic and planktonic foraminifera ages, suggesting minimal reworking. Furthermore, based on the occurrence of measurable radiocarbon in cores from beneath multiple modern ice streams, Kingslake et al. (2018) simulate a similarly timed

minimum in grounding-line location followed by a readvance to modern extent. We show an estimated grounding line, taken from the minimum estimate presented by Greenwood et al. (2018), at the 8 cal ka BP timestep, but recognize that the retreat event could have been larger in magnitude and earlier (McKay et al., 2016; Kingslake et al., 2018).

The composite grounding-zone wedge itself appears to have formed over a ~3–4 kyr timespan if the previous grounding-line minimum occurred at ~8 cal ka BP. The basal grounding-zone wedge (GZW1; Fig. 9d) yields a grounding-line retreat age of 5.8 cal ka BP (KC28, Table 2). It is unclear how far the grounding line retreated before readvancing to form the top grounding-zone wedge (GZW2; Fig. 9d), but the final grounding-line retreat from the composite wedge occurred at ~4.3 cal ka BP (KC04, Table 2). This

timing is consistent with far-field sea level observations that suggest the majority of Antarctic ice sheet melting ceased by ~4 ka (Yokoyama et al., 2012; 2016b; 2019).

5.3. Deglacial history (4 cal ka – present)

In spite of careful evaluation of new and previously-published ages, constraints on ice retreat from the southwestern Ross Sea are inconsistent with geomorphology. Backstepping grounding-zone wedges and moraines suggest that after the ~4 cal ka BP culmination of the readvance, ice retreated west into Transantarctic Mountain outlets and also onto Crary Bank from all sides (Fig. 9b, e-f), leading to the establishment of a semi-independent deglacial emergent ice rise fed by David Glacier (Halberstadt et al., 2016; Greenwood et al., 2018) that maintained an ice shelf until ~1.6 cal ka BP (KC04, Table 2). Although geomorphic reconstructions (Lee et al., 2017; Halberstadt et al., 2016; Greenwood et al., 2018) suggest southern Drygalski Trough was the last area to deglaciate, grounding-line and ice shelf retreat ages from this region are far older than expected (Fig. 7d). Because higher confidence is given to most outer and middle continental shelf ages and less to inner continental shelf ages, we heavily depend on interpretation of retreat patterns from geomorphology in the southwestern Ross Sea to complete our story. The reorganization and readvance of ice flowing from the Transantarctic Mountains into JOIDES Trough requires that ice remain grounded in southern Drygalski Trough during this time (Greenwood et al., 2018). If we only based our reconstruction on ages from this region, we would show southern Drygalski Trough becoming open marine starting at ~7 cal ka BP (NBP1502A KC44). However, our high confidence ages suggest a major ice-shelf collapse occurred after 9 cal ka BP, and it would be glaciologically difficult for ice to have reorganized and readvanced accordingly in such a short timeframe as 9–7 cal ka BP. As a result, Fig. 7f relies primarily on geomorphic reconstruction rather than ages for the region west of Crary Bank. While we are confident in our interpretations of open marine onset on the eastern flank of Crary Bank, we do not have enough grounding-line retreat ages to confirm the geomorphologic story. Therefore, the grounding-line retreat in Fig. 8e and f should be taken as relative, not absolute.

The reason for the older ages in southern Drygalski Trough is unclear. We note that surface ages (Fig. 4) are not anomalous, and Hall et al. (2010b) demonstrate the reservoir age has been relatively consistent for the southwestern Ross Sea for the past 6000 years. Instead, we suggest that until recently, when ice became less extensive, large amounts of relict carbon were present in the glacimarine environment. Southwestern Ross Sea is characterized by a thin veneer of unconsolidated glacial/glacimarine sediments overlying strata that are Miocene and older (Wong and Christoffel, 1981; Anderson, 1999). These older strata are likely sampled by outlet glaciers in the southwestern Ross Sea as they fluctuate through the Transantarctic Mountains and southern Drygalski Trough, causing strong inherent bias in radiocarbon ages. A possible test for this would be to investigate abundances of recycled palynomorphs in cores from southern Drygalski Trough, which was not included in previous studies of Ross Sea palynomorphs (Truswell and Drewry, 1984).

Regardless of what the radiocarbon record of events in southwestern Ross Sea may be, there are still gaps in the geomorphic story, particularly in McMurdo Sound. However, it is clear from Halberstadt et al. (2016) and the ages reported in this study that the banks strongly influenced the behavior of ice on the inner continental shelf in the late stages of ice sheet retreat. Rather than retreating as a ‘swinging gate’, the ice in the Ross Sea utilized the banks as pinning points for deglacial emergent ice rises. In this regard, our ages are broadly consistent with the Halberstadt et al.

(2016) retreat scenario (Fig. 2). With careful foraminiferal analysis such as ours, it is possible to obtain good radiocarbon dates. In the future, new technology may allow more widespread opportunities for accurate dating of small volumes of foraminifera or compound-specific organic matter from glacial environments.

5.4. Terrestrial and marine relationships

Sea level records from raised beaches along the Transantarctic Mountains are used to determine ice unloading history. Beginning with the work of Conway et al. (1999), terrestrial records (e.g., Hall et al., 2013) have been extrapolated across the Ross Sea to broadly interpret deglacial history. Terrestrial and marine record discrepancies (Anderson et al., 2014) and modelling studies for various Antarctic glacier systems show a slight lag in upstream terrestrial response to marine grounding-line retreat (Payne et al., 2004; Favier et al., 2014; Jougin et al., 2014; Jones et al., 2015). Recently published multibeam data (Halberstadt et al., 2016) and core records (McKay et al., 2016) suggest the central Ross Sea deglaciated prior to the coastal area adjacent to the Transantarctic Mountains and that the terrestrial records represent the retreat of local outlet glaciers.

Cores (KC37, GC1604, GC28; Table 2) near Terra Nova Bay show open marine onset at ~9.5 cal ka BP, which can be interpreted as a minimum age of grounding-line retreat and roughly agrees with the timing of nearby terrestrial thinning that occurred by 8 cal ka BP (Baroni and Hall et al., 2004). However, because geomorphic reconstructions (Halberstadt et al., 2016; Greenwood et al., 2018) indicate that the majority of the northern Victoria Land outlet glaciers have little connection to any ice streams other than the one that once flowed through northern Drygalski Trough, we cannot use the Terra Nova Bay terrestrial record to infer anything about broader ice sheet retreat across the Ross Sea.

Other terrestrial records in southern Victoria Land near Ross Island suggest grounded ice thinned to present levels by 7.8 cal ka BP (Hall et al., 2004, 2013). We find that two large troughs (JOIDES and Pennell) experienced major, though complex, retreat nearly concurrent with terrestrial changes. David Glacier and outlet glaciers to the south have been shown to have significant contributions to ice flow through JOIDES Trough and perhaps Pennell Trough (Lee et al., 2017; Halberstadt et al., 2016; Greenwood et al., 2018). We suggest that this source ice in southern Victoria Land near Ross Island was drawn down in response to the large-scale retreat and readvance in JOIDES Trough (section 5.2). Thus, the Hall et al. (2004, 2013) terrestrial record of thinning could reflect larger-scale western and central Ross Sea change. Furthermore, a new terrestrial record of initial thinning at ~12.3 cal ka BP in the McMurdo Sound region (Christ and Bierman, 2019) may be related to initial grounding line retreat of the ice streams in the western Ross Sea. However, marine chronological records in McMurdo Sound and southern Drygalski Trough are not yet detailed or accurate enough to provide calendar constraints on the existing geomorphic story (Lee et al., 2017; Halberstadt et al., 2016; Greenwood et al., 2018) or fully determine how reflective the terrestrial records are of the ice in the broader marine realm.

5.5. Dating practices moving forward

Ideally, we would have used all three dating analyses on single intervals to directly compare and evaluate the dating methods, as well as compare across different facies and locations. However, the availability of certain datable materials were unfortunately limited in many cases. Still, this study shows AIO ages and compound-specific ages can be used to determine open marine onset in most instances, and targeting grounding-zone wedge foresets for

carbonate ages can be useful for determining grounding-line retreat if the material is in situ. AIO ages are comparable to compound-specific ages in open marine sediments (Facies 5) as long as careful corrections are carried out; however, they appear to exhibit bias in relation to in situ carbonate in more proximal sediments (e.g., Facies 2–4). There are difficulties in obtaining reliable ages in ice-proximal sediments, such as the large volumes of sample needed to recover enough dateable material in compound-specific dating. In the eastern Ross Sea, compound-specific radiocarbon dating has been successfully conducted on sub-ice shelf sediments (Yokoyama et al., 2016a), but in this study, all attempts to date facies other than open marine in the western Ross Sea using this method were unsuccessful. More sensitive instrumentation may allow smaller samples sizes in the future, but in the meantime, alternative dating methods should be investigated.

Technology capable of analyzing extremely small quantities of carbonate exists (e.g., MICADAS; Synal et al., 2007), but care should be taken to ensure the chosen sample is in situ. Like compound-specific dating, ramped pyrolysis (Ramped PyrOx) offers another successful method of dating sediments where carbonate is not well-preserved and has been shown to significantly improve chronologies in Antarctic Peninsula cores from Lapeyrère Bay (Subt et al., 2016), Hugo Bay Trough (Rosenheim et al., 2013), and Palmer Deep (Rosenheim et al., 2008), with Ramped PyrOx ages appearing to be comparable or younger than carbonate ages in sub-ice shelf sediments (Subt et al., 2016), including diamictites (Subt et al., 2017). Ramped PyrOx has not yet been tested with respect to facies identified using a geomorphic framework, but could prove useful for establishing chronologies in ice-proximal sediments where (1) traditional dating of carbonate is insufficient due to reworking or mixing and (2) where organic carbon quantities are too small for compound-specific dating. Furthermore, our current method of performing an LCO-correction is based on the assumption that the LCO is consistent downcore, even though we know that organic matter varies through time (e.g., Domack and Ishman, 1993; Domack et al., 1995; Shevenell et al., 1996; Rosenheim et al., 2008; Michalchuk et al., 2009; Milliken et al., 2009). Our correlations between our AIO and compound-specific ages (e.g., Fig. 6) support the use of LCO-correction of open marine sediments (Facies 1) in this way, but this is likely not effective everywhere in Antarctica or for all facies. Rosenheim et al. (2013) demonstrate the variable downcore offset using the range of Ramped PyrOx measurements that represent the possible proportions of pre-aged carbon in each sample. In the future, innovative corrections utilizing this type of information may provide the best solutions for accurate dating.

6. Conclusions

We have made significant advances toward reconstructing an accurate ice sheet/ice shelf retreat history for the western Ross Sea by using a combination of geomorphic, sedimentologic, and micropaleontologic analyses to identify key sediment facies and transitions that mark grounding-line retreat and open-marine onset. By combining AIO, carbonate, and compound-specific dating of these transitions in NBP1502A cores and previously published ages that meet our criteria for reliability, we have added new calendar age constraints and greater detail to the marine record that corresponds with geomorphic reconstructions of post-LGM ice behavior. Using the range of ages from the proximal glacimarine sediments of the LGM grounding-zone wedges, we find that the ice reached its maximum extent at 25.6 cal ka BP and persisted for ~14 ky until 11.5 cal ka BP. In Pennell Trough, the maximum ice extent lasted for ~9 ky, from 24.2 to 15.1 cal ka BP. The

EAIS in both Pennell and JOIDES troughs began retreating around the same time as Meltwater Pulse 1A (MWP1a), but it is unlikely that the magnitude of ice loss from the western Ross Sea sector was great enough to be a significant contributor to sea level rise, as major changes did not occur until well after MWP1a. Subsequent retreat was complex, with deglacial emergent ice rises forming as grounded ice retreat onto banks. In JOIDES Trough, the ice shelf persisted until ~9.4 cal ka BP (KC48, Table 2) before a major-ice shelf collapse ensued, causing thick icebergs to calve from the grounding line to carve deep iceberg furrows into the seafloor across mid-JOIDES Trough. This major loss of EAIS ice may be concurrent or somehow linked to the 200 km retreat of the WAIS grounding line in Whales Deep sometime after ~11.5 cal ka BP (Bart et al., 2018).

In conjunction with the ice-shelf collapse, the grounding-line receded nearly to Ross Island, triggering a reorganization of flow in Drygalski Trough that resulted in outlet glaciers along the Transantarctic Mountains flowing southward and eastward to readvance northward into JOIDES Trough, with eventual retreat westward. This observation has at last aligned terrestrial and marine records of grounding-line retreat for the southern Drygalski region. The ice-shelf collapse (~9 cal ka BP) and readvance (until ~4 cal ka BP) of Transantarctic outlet glaciers was a likely cause of the thinning of terrestrial ice at ~7.8 cal ka BP along the southern Scott Coast (Hall et al., 2004). An ice shelf covering southern JOIDES and Central Basin persisted subsequent to retreat onto Crary Bank and into the Transantarctic outlet glaciers. Here, grounding-line retreat is best documented by geomorphology as radiocarbon ages from the area have significant age biases.

We demonstrate that, in general, AIO ages are reliable in open marine sediments, excluding IRD-rich intervals, by showing good agreement with compound-specific ages (Fig. 6). It is clear from Fig. 4 that careful selection of seemingly in-situ foraminifera for radiocarbon dating can still result in suspiciously old ages in ice-proximal sediments. However, ages obtained in this way are likely more reliable than analyzing foraminifera without regard for reworking. Thus, it is imperative that some level of detailed foraminiferal analysis is performed unless analyzing small quantities of definitively pristine foraminifera (e.g., MICADAS; Synal et al., 2007). Compound-specific and Ramped PyrOx methods represent significant improvements toward eliminating biased results. Regardless of technological advancements, radiocarbon ages should not be taken at face value, but should be interpreted with careful consideration of geomorphic indicators of ice behavior and depositional environments, sedimentary facies from which ages are extracted, and potential for bias from relict organic carbon or recycled carbonate material. With this approach, we have made substantial strides toward reconstructing the marine record of ice-sheet and ice-shelf retreat in the western Ross Sea to a fine scale, and have begun to link marine and terrestrial records whose relationships have previously been poorly understood.

Acknowledgments

We thank the crew of the RV/IB Nathaniel B. Palmer, the Antarctic Support Contract personnel, and ship-based scientists for their efforts toward a successful expedition. We thank A. Fonseca and B. Fowler for laboratory assistance, and C. Sjunneskog and S. Petrushak of the FSU Antarctic Research Facility for geotechnical assistance. This manuscript was greatly improved by the comments and suggestions of two reviewers—Brad Rosenheim and one anonymous reviewer. This work was funded by the National Science Foundation [NSF-PLR 1246353] to J.B.A., the National Science Centre of Poland [NCN-2015/17/B/ST10/03346] to W.M., and the Japan Society for the Promotion of Science KAKENHI [15KK0151, 17H01168] to Y.Y.

Appendix A. Supplementary data

Supplementary data to this article can be found online at <https://doi.org/10.1016/j.quascirev.2020.106166>.

References

- Ackert, R., 2008. Swinging gate or Saloon doors: Do we need a new model of Ross Sea deglaciation? Fifteenth West Antarctic Ice Sheet Meeting, Sterling, Virginia 811.
- Alley, R.B., Anandakrishnan, S., Dupont, T.K., Parizek, B.R., Pollard, D., 2007. Effect of sedimentation on ice-sheet grounding-line stability. *Science* 315 (5820), 1838–1841.
- Anderson, B., Hindmarsh, R.C., Lawson, W., 2004. A modelling study of the response of Hatherton Glacier to Ross Ice Sheet grounding line retreat. *Glob. Planet. Chang.* 42, 143–153.
- Anderson, J.B., 1999. Antarctic Marine Geology. Cambridge University Press.
- Anderson, J.B., Brake, C.F., Myers, N.C., 1984. Sedimentation in the Ross Sea, Antarctica. *Mar. Geol.* 57, 295–333.
- Anderson, J.B., Conway, H., Bart, P.J., Witus, A.E., Greenwood, S.L., McKay, R.M., Hall, B.L., Ackert, R.P., Licht, K., Jakobsson, M., Stone, J.O., 2014. Ross Sea paleo-ice sheet drainage and deglacial history during and since the LGM. *Quat. Sci. Rev.* 100, 31–54.
- Anderson, J.B., Kurtz, D.D., Domack, E.W., Balshaw, K.M., 1980. Glacial and glacial marine sediments of the Antarctic continental shelf. *J. Geol.* 88 (4), 399–414.
- Anderson, J.B., Shipp, S.S., Lowe, A.L., Wellner, J.S., Mosola, A.B., 2002. The antarctic ice sheet during the last glacial maximum and its subsequent retreat history: a review. *Quat. Sci. Rev.* 21, 49–70.
- Andrews, J.T., Domack, E.W., Cunningham, W.L., Leventer, A., Licht, K.J., Jull, A.T., DeMaster, D.J., Jennings, A.E., 1999. Problems and possible solutions concerning radiocarbon dating of surface marine sediments, Ross Sea, Antarctica. *Quat. Res.* (Orlando) 52 (2), 206–216.
- Baroni, C., Hall, B.L., 2004. A new Holocene relative sea-level curve for Terra Nova bay, Victoria Land, Antarctica. *J. Quat. Sci.* 19, 377–396.
- Bart, P.J., Cone, A.N., 2012. Early stall of West Antarctic Ice Sheet advance on the eastern Ross Sea middle shelf followed by retreat at 27,500 14 C yr BP. *Palaeogeogr. Palaeocl.* 335, 52–60.
- Bart, P.J., Coquereau, L., Warny, S., Majewski, W., 2016. In situ foraminifera in grounding zone diamict: a working hypothesis. *Antarct. Sci.* 28 (4), 313–321.
- Bart, P.J., DeCesare, M., Rosenheim, B.E., Majewski, W., McGlennan, A., 2018. A centuries-long delay between a paleo-ice-shelf collapse and grounding-line retreat in the Whales Deep Basin, eastern Ross Sea, Antarctica. *Sci. Rep.* 8 (1), 12392.
- Batchelor, C.L., Dowdeswell, J.A., 2015. Ice-sheet grounding-zone wedges (GZWs) on high-latitude continental margins. *Mar. Geol.* 363, 65–92.
- Bentley, M.J., et al., 2014. A community-based geological reconstruction of antarctic ice sheet deglaciation since the last glacial maximum. *Quat. Sci. Rev.* 100, 1–9.
- Berkman, P.A., Forman, S.L., 1996. Pre-bomb radiocarbon and the reservoir correction for calcareous marine species in the Southern Ocean. *Geophys. Res. Lett.* 23 (4), 363–366.
- Bockheim, J., Wilson, S.C., Denton, G.H., Andersen, B.G., Stuiver, M., 1989. Late quaternary ice-surface fluctuations of Hatherton Glacier, transantarctic Mountains. *Quat. Sci. Rev.* 31, 229–254.
- Boulton, G.S., 1986. Push-moraines and glacier-contact fans in marine and terrestrial environments. *Sedimentology* 33 (5), 677–698.
- Bromley, G.R., Hall, B.L., Stone, J.O., Conway, H., 2012. Late Pleistocene evolution of Scott Glacier, southern Transantarctic Mountains: implications for the Antarctic contribution to deglacial sea level. *Quat. Sci. Rev.* 50, 1–13.
- Brook, E.J., Kurz, M.D., Ackert, R.P., Raisbeck, G., Yiou, F., 1995. Cosmogenic nuclide exposure ages and glacial history of late Quaternary Ross Sea drift in McMurdo Sound, Antarctica. *Earth Plan. Sci. Lett.* 131 (1–2), 41–56.
- Christ, A.J., Bierman, P.R., 2019. The local last glacial maximum in McMurdo Sound, Antarctica: implications for ice-sheet behavior in the Ross Sea embayment. *Geol. Soc. Am. Bull.* 132 (1–2), 31–47.
- Christiansen, K., Jacobel, R.W., Horgan, H.J., Alley, R.B., Anandakrishnan, S., Holland, D.M., DallaSantta, K.J., 2016. Basal conditions at the grounding zone of Whillans Ice Stream, West Antarctica, from ice-penetrating radar. *J. Geophys. Res.: Earth Surf.* 121 (11), 1954–1983.
- Clark, P.U., Dyke, A.S., Shakun, J.D., Carlson, A.E., Clark, J., Wohlfarth, B., Mitrovica, J.X., Hostetler, S.W., McCabe, A.M., 2009. The last glacial maximum. *Science* 325, 710–714.
- Clayton-Greene, J., Hendy, C., Hogg, A., 1988. Chronology of a Wisconsin age proglacial lake in the Miers Valley, Antarctica. *N. Z. J. Geol. Geophys.* 31, 353–361.
- Conway, H., Hall, B.L., Denton, G.H., Gades, A.M., Waddington, E.D., 1999. Past and future grounding-line retreat of the west antarctic ice sheet. *Science* 286, 280–283.
- Cowan, E.A., Christoffersen, P., Powell, R.D., 2012. Sedimentological signature of a deformable bed preserved beneath an ice stream in a Late Pleistocene glacial sequence, Ross Sea, Antarctica. *J. Sediment. Res.* 82 (4), 270–282.
- Cunningham, W.L., Leventer, A., Andrews, J.T., Jennings, A.E., Licht, K.J., 1999. Late Pleistocene-Holocene marine conditions in the Ross Sea, Antarctica: evidence from the diatom record. *Holocene* 9 (2), 129–139.
- DeConto, R.M., Pollard, D., 2016. Contribution of Antarctica to past and future sea-level rise. *Nature* 531 (7596), 591–597.
- DeMaster, D.J., Ragueneau, O., Nittrouer, C.A., 1996. Preservation efficiencies and accumulation rates for biogenic silica and organic C, N, and P in high-latitude sediments: the Ross Sea. *J. Geophys. Res.: Oceans* 101 (C8), 18501–18518.
- Domack, E., Ambles, D., Gilbert, R., Brachfeld, S., Camerlenghi, A., Rebesco, M., Canals, M., Urgeles, R., 2006. Subglacial morphology and glacial evolution of the Palmer deep outlet system, Antarctic Peninsula. *Geomorphology* 75 (1–2), 125–142.
- Domack, E.W., Ishman, S., 1993. Oceanographic and physiographic controls on modern sedimentation within Antarctic fjords. *Geol. Soc. Am. Bull.* 105 (9), 1175–1189.
- Domack, E.W., Ishman, S.E., Stein, A.B., McClenen, C.E., Jull, A.T., 1995. Late Holocene advance of the müller ice shelf, antarctic Peninsula: sedimentological, geochemical and palaeontological evidence. *Antarct. Sci.* 7 (2), 159–170.
- Domack, E.W., Jacobson, E.A., Shipp, S., Anderson, J.B., 1999. Late pleistocene–holocene retreat of the west antarctic ice-sheet system in the Ross Sea: Part 2—sedimentologic and stratigraphic signature. *Geol. Soc. Am. Bull.* 111 (10), 1517–1536.
- Dowdeswell, J.A., Fugelli, E.M.G., 2012. The seismic architecture and geometry of grounding-zone wedges formed at the marine margins of past ice sheets. *Geol. Soc. Am. Bull.* 124 (11–12), 1750–1761.
- Dunbar, R.B., Anderson, J.B., Domack, E.W., Jacobs, S.S., 1985. Oceanographic influences on sedimentation along the Antarctic continental shelf. In: Jacobs, S.S. (Ed.), Oceanology of the Antarctic Continental Shelf, pp. 291–312.
- Eglington, T.I., Aluwihare, L.I., Bauer, J.E., Druffel, E.R., McNichol, A.P., 1996. Gas chromatographic isolation of individual compounds from complex matrices for radiocarbon dating. *Anal. Chem.* 68 (5), 904–912.
- Favier, L., Durand, G., Cornford, S.L., Gudmundsson, G.H., Gagliardini, O., Gillet-Chaulet, F., Zwinger, T., Payne, A.J., Le Brocq, A.M., 2014. Retreat of Pine Island Glacier controlled by marine ice-sheet instability. *Nat. Clim. Chang.* 4 (2), 117–121.
- Folk, R.L., Ward, W.C., 1957. Brazos River bar: a study in the significance of grain size parameters. *J. Sediment. Res.* 27 (1), 3–26.
- Fretwell, P., Pritchard, H.D., Vaughan, D.G., Bamber, J.L., Barrand, N.E., Bell, R., Bianchi, C., Bingham, R.G., Blankenship, D.D., Casassa, G., Catania, G., Callens, D., Conway, H., Cook, A.J., Corr, H.F.J., Damaske, D., Damm, V., Ferraccioli, F., Forsberg, R., Fujita, S., Gim, Y., Gogineni, P., Griggs, J.A., Hindmarsh, R.C.A., Holmlund, P., Holt, J.W., Jacobel, R.W., Jenkins, A., Jokat, W., Jordan, T., King, E.C., Kohler, J., Krabill, W., Riger-Kusk, M., Langley, K.A., Leitchenkov, G., Leuschen, C., Luyendyk, B.P., Matsuoka, K., Mouginot, J., Nitsche, F.O., Nogi, Y., Nost, O.A., Popov, S.V., Rignot, E., Rippin, D.M., Rivera, A., Roberts, J., Ross, N., Siegert, M.J., Smith, A.M., Steinhage, D., Studinger, M., Sun, B., Tinto, B.K., Welch, B.C., Wilson, D., Young, D.A., Xiangbin, C., Zirizzotti, A., 2013. Bedmap2: improved ice bed, surface and thickness datasets for Antarctica. *Cryosphere* 7 (1), 4305–4361.
- Colledge, N.R., Fogwill, C.J., Mackintosh, A.N., Buckley, K.M., 2012. Dynamics of the last glacial maximum Antarctic ice-sheet and its response to ocean forcing. *P. Nat. A. Sci.* 109 (40), 16052–16056.
- Colledge, N.R., Kowalewski, D.E., Naish, T.R., Levy, R.H., Fogwill, C.J., Gasson, E.G., 2015. The multi-millennial Antarctic commitment to future sea-level rise. *Nature* 526 (7573), 421–425.
- Colledge, N.R., Levy, R.H., McKay, R.M., Naish, T.R., 2017. East Antarctic Ice Sheet most vulnerable to Weddell Sea warming. *Geophys. Res. Lett.* 44 (5), 2343–2351.
- Greenwood, S.L., Simkins, L.M., Halberstadt, A.R.W., Prothro, L.O., Anderson, J.B., 2018. Holocene reconfiguration and readvance of the east antarctic ice sheet. *Nat. Commun.* 9.
- Gulick, S.P., Shevenell, A.E., Montelli, A., Fernandez, R., Smith, C., Warny, S., Bohaty, S.M., Sjunneskog, C., Leventer, A., Frederick, B., Blankenship, D.D., 2017. Initiation and long-term instability of the east antarctic ice sheet. *Nature* 552 (7684), 225–229.
- Halberstadt, A.R.W., Simkins, L.M., Anderson, J.B., Prothro, L.O., Bart, P.J., 2018. Characteristics of the deforming bed: till properties on the deglaciated Antarctic continental shelf. *J. Glaciol.* 64 (248), 1014–1027.
- Halberstadt, A.R.W., Simkins, L.M., Greenwood, S.L., Anderson, J.B., 2016. Past ice-sheet behaviour: retreat scenarios and changing controls in the Ross Sea, Antarctica. *Cryosphere* 10 (3), 1003–1020.
- Hall, B.L., Denton, G.H., 2000. Radiocarbon chronology of Ross Sea drift, eastern Taylor Valley, Antarctica: evidence for a grounded ice sheet in the Ross Sea at the last glacial maximum. *Geogr. Ann.* 82A, 305–336.
- Hall, B.L., Denton, G.H., Baroni, C., 2004. Holocene relative sea-level history of the southern Victoria Land coast, Antarctica. *Glob. Planet. Chang.* 42, 241–263.
- Hall, B.L., Denton, G.H., Fountain, A.G., Hendy, C., Henderson, G., 2010a. Antarctic lakes suggest millennial reorganizations of Southern Hemisphere atmospheric and oceanic circulation. *Proc. Natl. Acad. Sci.* 107, 21355–21359.
- Hall, B.L., Denton, G.H., Stone, J.O., Conway, H., 2013. History of the grounded ice sheet in the Ross Sea sector of Antarctica during the last glacial maximum and the last termination. In: Geological Society of London. Special Publication, pp. 381–385. <https://doi.org/10.1144/SP381.5>.
- Hall, B.L., Henderson, G.M., Baroni, C., Kellogg, T.B., 2010b. Constant Holocene Southern-Ocean 14C reservoir ages and ice-shelf flow rates. *Earth Planet. Sci. Lett.* 296 (1–2), 115–123.
- Hauer, M.E., Evans, J.M., Mishra, D.R., 2016. Millions projected to be at risk from sea-level rise in the continental United States. *Nat. Clim. Chang.* 6 (7), 691–695.
- Hillenbrand, C.D., Smith, J.A., Kuhn, G., Esper, O., Gersonde, R., Larter, R.D., Maher, B.,

- Moreton, S.G., Shimmield, T.M., Korte, M., 2010. Age assignment of a diatomaceous ooze deposited in the western amundsen Sea Embayment after the last glacial maximum. *J. Quat. Sci.* 25 (3), 280–295.
- Hirabayashi, S., Yokoyama, Y., Suzuki, A., Miyairi, Y., Aze, T., 2017. Multidecadal oceanographic changes in the western Pacific detected through high-resolution bomb-derived radiocarbon measurements on corals. *Geochem. Geophys. Geosyst.* 18 (4), 1608–1617.
- Hogan, K.A., Cofaigh, C.O., Jennings, A.E., Dowdeswell, J.A., Hiemstra, J.F., 2016. Deglaciation of a major palaeo-ice stream in disko trough, west Greenland. *Quat. Sci. Rev.* 147, 5–26.
- Ingalls, A.E., Pearson, A., 2005. Ten years of compound-specific radiocarbon analysis. *Oceanography* 18 (3), 18–31.
- Ishikawa, N.F., Itahashi, Y., Blattmann, T.M., Takano, Y., Ogawa, N.O., Yamane, M., Yokoyama, Y., Nagata, T., Yoneda, M., Haghipour, N., Eglinton, T.I., 2018. Improved method for isolation and purification of underivatized amino acids for radiocarbon analysis. *Anal. Chem.* 90 (20), 12035–12041.
- Jacobs, S.S., Bauer, E.B., Bruchhausen, P.M., Gordon, A.L., Root, T.F., Rosselot, F.L., 1974. Eltanin report. Cruises 47–50, 1971, 52–55, 1972. Lamont-Doherty Geological Observatory of Columbia University Technical Report CU-2-74.
- Jones, R.S., Mackintosh, A.N., Norton, K.P., Golledge, N.R., Fogwill, C.J., Kubik, P.W., Christl, M., Greenwood, S.L., 2015. Rapid Holocene thinning of an East Antarctic outlet glacier driven by marine ice sheet instability. *Nat. Commun.* 6, 8910.
- Joughin, I., Smith, B.E., Medley, B., 2014. Marine ice sheet collapse potentially under way for the Thwaites Glacier Basin, West Antarctica. *Science* 344 (6185), 735–738.
- Kellogg, D.E., Kellogg, T.B., 1986. Diatom biostratigraphy of sediment cores from beneath the Ross ice shelf. *Micropaleontology* 74–94.
- Kellogg, T.B., Kellogg, D.E., 1988. Antarctic cryogenic sediments: biotic and inorganic facies of ice shelf and marine-based ice sheet environments. *Palaeogeogr. Palaeoclimatol. Palaeoecol.* 67 (1–2), 51–74.
- Kennett, J.P., 1968. The Fauna of the Ross Sea: Part 6: Ecology and Distribution of Foraminifera. Department of Scientific and Industrial Research.
- Kingslake, J., Scherer, R.P., Albrecht, T., Coenen, J., Powell, R.D., Reese, R., Stansell, N.D., Tulaczek, S., Wearing, M.G., Whitehouse, P.L., 2018. Extensive retreat and re-advance of the West Antarctic ice sheet during the Holocene. *Nature* 558 (7710), 430–434.
- Larter, R.D., Vanneste, L.E., 1995. Relict subglacial deltas on the Antarctic Peninsula outer shelf. *Geology* 23 (1), 33–36.
- Lee, J.I., McKay, R.M., Colledge, N.R., Yoon, H.I., Yoo, K.C., Kim, H.J., Hong, J.K., 2017. Widespread persistence of expanded East Antarctic glaciers in the southwest Ross Sea during the last deglaciation. *Geology* 45 (5), 403–406.
- Leventer, A., Domack, E., Dunbar, R., Pike, J., Stickley, C., Maddison, E., Brachfeld, S., Manley, P., McClenen, C., 2006. Marine sediment record from the East Antarctic margin reveals dynamics of ice sheet recession. *GSA Today (Geol. Soc. Am.)* 16 (12), 4–10.
- Licht, K.J., Andrews, J.T., 2002. The 14 C record of Late Pleistocene ice advance and retreat in the central Ross Sea, Antarctica. *Arctic Antarct. Alpine Res.* 324–333.
- Licht, K.J., Dunbar, N.W., Andrews, J.T., Jennings, A.E., 1999. Distinguishing subglacial till and glacial marine diamictons in the western Ross Sea, Antarctica: implications for a last glacial maximum grounding line. *Geol. Soc. Am. Bull.* 111 (1), 91–103.
- Licht, K.J., Jennings, A.E., Andrews, J.T., Williams, K.M., 1996. Chronology of late Wisconsin ice retreat from the western Ross Sea, Antarctica. *Geology* 24 (3), 223–226.
- Livingstone, S.J., Cofaigh, C.O., Stokes, C.R., Hillenbrand, C.D., Vieli, A., Jamieson, S.S.R., 2012. Antarctic palaeo-ice streams. *Earth Sci. Rev.* 111, 90–128.
- Mackintosh, A., Golledge, N., Domack, E., Dunbar, R., Leventer, A., White, D., Pollard, D., DeConto, R., Fink, D., Zwart, D., Gore, D., 2011. Retreat of the East Antarctic Ice Sheet during the last glacial termination. *Nat. Geosci.* 4 (3), 195–202.
- Majewski, W., Bart, P.J., McGlannan, A.J., 2018. Foraminiferal assemblages from ice-proximal paleo-settings in the Whales deep basin, eastern Ross Sea, Antarctica. *Palaeogeogr. Palaeoclimatol. Palaeoecol.* 493, 64–81.
- Matsuoka, K., Hindmarsh, R.C., Moholdt, G., Bentley, M.J., Pritchard, H.D., Brown, J., Conway, H., Drews, R., Durand, G., Goldberg, D., Hattermann, T., 2015. Antarctic ice rises and rumples: their properties and significance for ice-sheet dynamics and evolution. *Earth Sci. Rev.* 150, 724–745.
- Mayewski, P.A., Meredith, M.P., Summerhayes, C.P., Turner, J., Worby, A., Barrett, P.J., Casassa, G., Bertler, N.A.N., Bracegirdle, T., Naveira Garabato, A.C., Bromwich, D.H., Campbell, H., Hamilton, G.S., Lyons, W.B., Maasch, K.A., Aoki, S., Xiao, C., van Ommen, T., 2009. State of the antarctic and Southern Ocean climate system. *Rev. Geophys.* 47, RG1003.
- McGlannan, A.J., Bart, P.J., Chow, J.M., DeCesare, M., 2017. On the influence of post-LGM ice shelf loss and grounding zone sedimentation on West Antarctic ice sheet stability. *Mar. Geol.* 392, 151–169.
- McKay, R.M., Dunbar, G.B., Naish, T.R., Barrett, P.J., Carter, L., Harper, M., 2008. Retreat history of the Ross ice sheet (shelf) since the last glacial maximum from deep-basin sediment cores around Ross Island. *Palaeogeogr. Palaeoclimatol. Palaeoecol.* 260 (1), 245–261.
- McKay, R., Golledge, N.R., Maas, S., Naish, T., Levy, R., Dunbar, G., Kuhn, G., 2016. Antarctic marine ice-sheet retreat in the Ross Sea during the early Holocene. *Geology* 44 (1), 7–10.
- Mezgec, K., Stenni, B., Crosta, X., Masson-Delmotte, V., Baroni, C., Braida, M., Ciardini, V., Colizza, E., Melis, R., Salvatore, M.C., Severi, M., 2017. Holocene sea ice variability driven by wind and polynya efficiency in the Ross Sea. *Nat. Commun.* 8 (1), 1334.
- Michalchuk, B.R., Anderson, J.B., Wellner, J.S., Manley, P.L., Majewski, W., Bohaty, S., 2009. Holocene climate and glacial history of the northeastern Antarctic Peninsula: the marine sedimentary record from a long SHALDRIL core. *Quat. Sci. Rev.* 28 (27–28), 3049–3065.
- Milam, R.W., Anderson, J.B., 1981. Distribution and ecology of recent benthonic foraminifera of the adelie-george-V continental-shelf and slope, Antarctica. *Mar. Micropaleontol.* 6 (3), 297–325.
- Milliken, K.T., Anderson, J.B., Wellner, J.S., Bohaty, S.M., Manley, P.L., 2009. High-resolution Holocene climate record from maxwell bay, south shetland Islands, Antarctica. *GSA Bull.* 121 (11–12), 1711–1725.
- Minzoni, R.T., Majewski, W., Anderson, J.B., Yokoyama, Y., Fernandez, R., Jakobsson, M., 2017. Oceanographic influences on the stability of the cosgrove ice shelf, Antarctica. *Holocene* 27 (11), 1645–1658.
- Morris, E.M., Vaughan, D.G., 2003. Antarctic Research series: antarctic Peninsula climate variability, hist. *Paleoenviron. Perspect.* 79, 61–68.
- Mosola, A.B., Anderson, J.B., 2006. Expansion and rapid retreat of the West Antarctic Ice Sheet in eastern Ross Sea: possible consequence of over-extended ice streams? *Quat. Sci. Rev.* 25 (17), 2177–2196.
- Ohkouchi, N., Eglinton, T.I., Hayes, J.M., 2003. Radiocarbon dating of individual fatty acids as a tool for refining Antarctic margin sediment chronologies. *Radiocarbon* 45 (1), 17–24.
- Ottesen, D., Dowdeswell, J.A., 2006. Assemblages of submarine landforms produced by tidewater glaciers in Svalbard. *J. Foraminifer. Res.: Earth Surf.* 111 (F1), F01016.
- Ottesen, D., Dowdeswell, J.A., Rise, L., 2005. Submarine landforms and the reconstruction of fast-flowing ice streams within a large Quaternary ice sheet: the 2500-km-long Norwegian-Svalbard margin (57–80°N). *GSA Bull.* 117 (7–8), 1033–1050.
- Payne, A.J., Vieli, A., Shepherd, A.P., Wingham, D.J., Rignot, E., 2004. Recent dramatic thinning of largest West Antarctic ice stream triggered by oceans. *Geophys. Res. Lett.* 31 (23), L23401.
- Pillsbury, R.D., Jacobs, S.S., 1985. Preliminary observations from long-term current meter moorings near the Ross Ice Shelf, Antarctica. *Oceanol. Antarct. Cont. Shelf* 43, 87–107.
- Powell, R.D., Dawber, M., McInnes, J.N., Pyne, A.R., 1996. Observations of the grounding-line area at a floating glacier terminus. *Ann. Glaciol.* 22, 217–223.
- Prothro, L.O., Simkins, L.M., Majewski, W., Anderson, J.B., 2018. Glacial retreat patterns and processes determined from integrated sedimentology and geomorphology records. *Mar. Geol.* 395, 104–119.
- Reimer, P.J., Bard, E., Bayliss, A., Beck, J.W., Blackwell, P.G., Ramsey, C.B., Buck, C.E., Cheng, H., Edwards, R.L., Friedrich, M., Grootes, P.M., 2013. IntCal13 and Marine13 radiocarbon age calibration curves 0–50,000 years cal BP. *Radiocarbon* 55 (4), 1869–1887.
- Ritz, C., Edwards, T.L., Durand, G., Payne, A.J., Peyaud, V., Hindmarsh, R.C., 2015. Potential sea-level rise from Antarctic ice-sheet instability constrained by observations. *Nature* 528 (7580), 115–118.
- Rosenheim, B.E., Day, M.B., Domack, E., Schrum, H., Benthen, A., Hayes, J.M., 2008. Antarctic sediment chronology by programmed-temperature pyrolysis: methodology and data treatment. *Geochem. Geophys. Geosyst.* 9 (4), Q04005.
- Rosenheim, B.E., Santoro, J.A., Gunter, M., Domack, E.W., 2013. Improving Antarctic sediment 14 C dating using ramped pyrolysis: an example from the Hugo Island trough. *Radiocarbon* 55 (1), 115–126.
- Salvi, C., Busetti, M., Marinoni, L., Brambati, A., 2006. Late quaternary glacial marine to marine sedimentation in the Pennell Trough (Ross Sea, Antarctica). *Palaeogeogr. Palaeoclimatol. Palaeoecol.* 231 (1–2), 199–214.
- Schoof, C., 2007. Ice sheet grounding line dynamics: steady states, stability, and hysteresis. *J. Geophys. Res.: Earth Surf.* 112 (F3).
- Schuerch, M., Spencer, T., Temmerman, S., Kirwan, M.L., Wolff, C., Lincke, D., McOwen, C.J., Pickering, M.D., Reef, R., Vafeidis, A.T., Hinkel, J., 2018. Future response of global coastal wetlands to sea-level rise. *Nature* 561 (7722), 231–234.
- Shepherd, A., Wingham, D., Rignot, E., 2004. warm ocean is eroding West Antarctic ice sheet. *Geophys. Res. Lett.* 31, L23402.
- Shevenell, A.E., Domack, E.W., Kernan, G.M., 1996. Record of Holocene paleoclimate change along the Antarctic Peninsula: evidence from glacial marine sediments, Lallemand Fjord. In: Papers and Proceedings of the Royal Society of Tasmania, vol 130, pp. 55–64, 2.
- Shipp, S., Anderson, J.B., Domack, E.W., 1999. Seismic signature of the late pleistocene fluctuation of the west antarctic ice sheet system in Ross Sea: a new perspective, Part I. *GSA Bull.* 111, 1486–1516.
- Simkins, L.M., Anderson, J.B., Greenwood, S.L., Gonnermann, H.M., Prothro, L.O., Halberstadt, A.R.W., Stearns, L.A., Pollard, D., DeConto, R.M., 2017. Anatomy of a meltwater drainage system beneath the ancestral East Antarctic Ice Sheet. *Nat. Geosci.* 10 (9), 691–697.
- Simkins, L.M., Greenwood, S.L., Anderson, J.B., 2018. Diagnosing ice sheet grounding line stability from landform morphology. *Cryosphere* 12 (8), 2707–2726. <https://doi.org/10.5194/tc-12-2707-2018>.
- Simkins, L.M., Simms, A.R., DeWitt, R., 2015. Assessing the link between coastal morphology, wave energy and sea ice throughout the Holocene from Antarctic raised beaches. *J. Quat. Sci.* 30 (4), 335–348.
- Smith Jr., W.O., Dinniman, M.S., Klinck, J.M., Hofmann, E., 2003. Biogeochemical climatologies in the Ross Sea, Antarctica: seasonal patterns of nutrients and biomass. *Deep Sea Res. Part II Top. Stud. Oceanogr.* 50 (22–26), 3083–3101.
- Spector, P., Stone, J., Cowdery, S.G., Hall, B., Conway, H., Bromley, G., 2017. Rapid

- early-holocene deglaciation in the Ross Sea, Antarctica: geophys. Res. Lett. 44 (15), 7817–7825. <https://doi.org/10.1002/2017GL074216>.
- Stone, J.O., Conway, H., Cowdery, S., Hall, B.L., Bromley, G.R., 2009. Deglaciation of the Ross Sea: the view from Scott and beardmore glaciers. In: 16th Annual West Antarctic Ice Sheet Meeting. Eatontown, Washington.
- Stuiver, M., Denton, G.H., Hughes, T., Fastook, J., 1981. History of the marine ice sheet in west Antarctica during the last glaciation. In: Denton, G., Hughes, T. (Eds.), *The Last Great Ice Sheets*. Wiley Interscience, New York, pp. 319–436.
- Stuiver, M., Reimer, P.J., 1993. Extended 14 C data base and revised CALIB 3.0 14 C age calibration program. Radiocarbon 35 (1), 215–230.
- Subt, C., Fangman, K.A., Wellner, J.S., Rosenheim, B.E., 2016. Sediment chronology in Antarctic deglacial sediments: reconciling organic carbon 14C ages to carbonate 14C ages using Ramped PyrOx. Holocene 26 (2), 265–273.
- Subt, C., Yoon, H.I., Yoo, K.C., Lee, J.I., Leventer, A., Domack, E.W., Rosenheim, B.E., 2017. Sub-ice shelf sediment geochronology utilizing novel radiocarbon methodology for highly detrital sediments. Geochem. Geophys. Geosy. 18 (4), 1404–1418.
- Synal, H.A., Stocker, M., Suter, M., 2007. MICADAS: a new compact radiocarbon AMS system. Nucl. Instrum. Methods Phys. Res. Sect. B Beam Interact. Mater. Atoms 259 (1), 7–13.
- Taviani, M., Reid, D.E., Anderson, J.B., 1993. Skeletal and isotopic composition and paleoclimatic significance of late Pleistocene carbonates, Ross Sea, Antarctica. J. Sediment. Res. 63 (1), 84–90.
- Todd, B.J., Valentine, P.C., Longva, O., Shaw, J., 2007. Glacial landforms on German Bank, Scotian Shelf: evidence for Late Wisconsinan ice-sheet dynamics and implications for the formation of De Geer moraines. Boreas 36 (2), 148–169.
- Todd, C., Stone, J.O., Conway, H., Hall, B.L., Bromley, G.R., 2010. Late quaternary evolution of Reedy Glacier, Antarctica. Quat. Sci. Rev. 29, 1328–1341.
- Truswell, E.M., Drewry, D.J., 1984. Distribution and provenance of recycled paly-nomorphs in surficial sediments of the Ross Sea, Antarctica. Mar. Geol. 59 (1–4), 187–214.
- Wilson, D.J., Bertram, R.A., Needham, E.F., van de Flierdt, T., Welsh, K.J., McKay, R.M., Mazumder, A., Riesselman, C.R., Jimenez-Espejo, F.J., Escutia, C., 2018. Ice loss from the east antarctic ice sheet during late pleistocene interglacials. Nature 561 (7723), 383–386.
- Winkelmann, R., Levermann, A., Ridgwell, A., Caldeira, K., 2015. Combustion of available fossil fuel resources sufficient to eliminate the Antarctic Ice Sheet. Sci. Adv. 1 (8), e1500589.
- Witus, A.E., Branecky, C.M., Anderson, J.B., Szczuciński, W., Schroeder, D.M., Blankenship, D.D., Jakobsson, M., 2014. Meltwater intensive glacial retreat in polar environments and investigation of associated sediments: example from Pine Island Bay, West Antarctica. Quat. Sci. Rev. 85, 99–118.
- Wong, H.K., Christoffel, D.A., 1981. A Reconnaissance Seismic Survey of McMurdo Sound and Terra Nova Bay, Ross Sea. Dry Valley Drilling Project, pp. 37–62.
- Yamane, M., Yokoyama, Y., Miyairi, Y., Suga, H., Matsuzaki, H., Dunbar, R.B., Ohkouchi, N., 2014. Compound-specific 14 C dating of IODP Expedition 318 core U1357A obtained off the Wilkes Land coast, Antarctica. Radiocarbon 56 (3), 1009–1017.
- Yokoyama, Y., Anderson, J.B., Yamane, M., Simkins, L.M., Miyairi, Y., Yamazaki, T., Koizumi, M., Suga, H., Kusahara, K., Prothro, L., Hasumi, H., Southon, J.R., Ohkouchi, N., 2016a. Widespread collapse of the Ross ice shelf during the late Holocene. Proc. Natl. Acad. Sci. 113 (9), 2354–2359.
- Yokoyama, Y., Esat, T.M., Thompson, W.G., Thomas, A.L., Webster, J.M., Miyairi, Y., Sawada, C., Aze, T., Matsuzaki, H., Okuno, J.I., Fallon, S., 2018. Rapid glaciation and a two-step sea level plunge into the Last Glacial Maximum. Nature 559 (7715), 603.
- Yokoyama, Y., Hirabayashi, S., Goto, K., Okuno, J., Sproson, A.D., Haraguchi, T., Ratnayake, N., Miyairi, Y., 2019. Holocene Indian Ocean sea level, Antarctic melting history and past tsunami deposits inferred using sea level reconstructions from Sri Lankan, Southeastern Indian and Maldivian coasts. Quat. Sci. Rev. 206, 150–161.
- Yokoyama, Y., Koizumi, M., Matsuzaki, H., Miyairi, Y., Ohkouchi, N., 2010. Developing ultra small-scale radiocarbon sample measurements at the University of Tokyo. Radiocarbon 52 (2), 310–318.
- Yokoyama, Y., Maeda, Y., Okuno, J.I., Miyairi, Y., Kosuge, T., 2016b. Holocene Antarctic melting and lithospheric uplift history of the southern Okinawa trough inferred from mid-to late-Holocene sea level in Iriomote Island, Ryukyu, Japan. Quat. Int. 397, 342–348.
- Yokoyama, Y., Miyairi, Y., Matsuzaki, H., Tsunomori, F., 2007. Relation between acid dissolution time in the vacuum test tube and time required for graphitization for AMS target preparation. Nucl. Instrum. Methods Phys. Res., Sect. B 259 (1), 330–334.
- Yokoyama, Y., Okuno, J.I., Miyairi, Y., Obrochta, S., Demboya, N., Makino, Y., Kawahata, H., 2012. Holocene sea-level change and Antarctic melting history derived from geological observations and geophysical modeling along the Shimokita Peninsula, northern Japan. Geophys. Res. Lett. 39 (13), L13502.